Acta Geochim (2025) 44:912–930
https://doi.org/10.1007/s11631-025-00772-z

ORIGINAL ARTICLE

# Petrogenesis and geodynamic setting of the Wutang granites in the Tong'an-Baishuidong lithium mining district, South China: Evidence from monazite U–Pb chronology, geochemistry, and Nd–Pb isotope

**Fushen Zhang[1] · Xiaotian Zhang[2] · Fangrong Zhang[1] · Yong Zhang[2] · Zhe Xu[1,2] · Xinyu Xu[2] · Jiayong Pan[2] · Fei Xia[2] · Guoqi Liu[2] · Yu Zhou[1,2] · Ying Liu[2] · Longmin Nie[1] · Fujun Zhong[2]**

Received: 29 April 2024 / Revised: 15 February 2025 / Accepted: 4 March 2025 / Published online: 27 March 2025


**Abstract** The Tong'an-Baishuidong mining district (TBMD), located in the eastern section of the Jiangnan Orogen, is a newly discovered granite-type lithium mining district. Thisstudy presents new monazite U–Pb chronological, whole-rock geochemical, and Nd–Pb isotopic data to reveal the petrogenesis and geodynamic setting of the Wutang granites in the TBMD. The monazite U–Pb age of 145.8 ± 1.0 Ma indicates that the granites were emplaced at the end of the Late Jurassic. Whole-rock geochemical results demonstrate that the Wutang granites are enriched in $SiO_2$ (72.80–73.40 wt%) but depleted in CaO (0.44–0.90 wt%) and MgO+$TiO_2$+TFeO (1.79–2.05 wt%). These granites exhibit negative Eu anomalies ($\delta$Eu = 0.3−0.4) and high aluminum saturation indexes (A/CNK = 1.2−1.6), differentiation indexes (DI = 90–92), and Rb/Sr ratios (4.7–8.1). They also have moderate Ba contents (239–278 ppm) and low Sr contents (52.7–82.0 ppm) as well as low Nb/Ta (2.2–5.3) and Zr/Hf (21.3–31.5) ratios. All these indicate that they are highly fractionated granites. Additionally, these granites contain 5–10 wt% muscovite but no hornblende, with calculated corundum contents of 2.3–5.5 wt%. They have low high-field strength element (HFSE) contents (Zr + Nb + Ce + Y = 182–202 ppm) and zircon saturation temperatures (700–770 °C), with Th and Y negatively linked with Rb. These petrographic and geochemical features further reveal that the Wutang granites belong to highly fractionated S-type granites. The $\varepsilon_{Nd}(t)$ values of these granites range from −9.03 to −8.23, corresponding to two-stage model ages ($T_{DM2}$) of 1488–1553 Ma. The initial Pb isotope ratios are: $(^{206}Pb/^{204}Pb)_i$ = 18.38–18.55, $(^{207}Pb/^{204}Pb)_i$ = 15.67–15.68, and $(^{208}Pb/^{204}Pb)_i$ = 38.62–38.67. These Nd–Pb isotopic results demonstrate that the parental magma originated from the partial melting of ancient crustal materials. In the meantime, the TBMD in the eastern section of the Jiangnan Orogen was in a

✉ Xiaotian Zhang
xtzhangeology@163.com

✉ Yong Zhang
zhangyong@ecut.edu.cn

Fushen Zhang
847326042@qq.com

Fangrong Zhang
420243911@qq.com

Zhe Xu
303543918@qq.com

Xinyu Xu
3032376442@qq.com

Jiayong Pan
jypan@ecut.edu.cn

Fei Xia
fxia@ecit.edu.cn

Guoqi Liu
liuguoqi@ecit.edu.cn

Yu Zhou
445426618@qq.com

Ying Liu
284915293@qq.com

Longmin Nie
448952259@qq.com

Fujun Zhong
zhongfujun@ecit.edu.cn

[1] Basic Geological Survey Institute, Jiangxi Geological Survey, and Exploration Institute, Nanchang 330030, China

[2] School of Earth Sciences, East China University of Technology, Jiangxi Province, Nanchang 330013, China

compression-extension transitional setting associated with the episodic subduction of the Paleo-Pacific Plate.

**Keywords** Wutang granites · Highly fractionated granites · Petrogenesis · Monazite U–Pb chronology · Tong'an-Baishuidong

## 1 Introduction

In the Mesozoic, the South China Plate was influenced by the Tethyan and Pacific tectonic domains, resulting in a world-renowned granitoid province, as well as enormous granite-related rare metal resources, such as tungsten, tin, lithium, beryllium, niobium, and tantalum (Mao et al. 2004, 2019; Hua et al. 2010; Chen et al. 2013; Xu et al. 2015; Zhao and Jiang 2022; Wu et al. 2023a, b). Multiple studies have demonstrated a close connection between highly fractionated granite and rare metal deposits in South China (e.g., Li et al. 2021; Hou et al. 2023; Ni et al. 2023). The enrichment of rare metals in highly fractionated granite is primarily controlled by the parent magma composition, partial melting degree, separation crystallization process, and fluid metasomatism (Linnen et al. 2012; Gou et al. 2023). Therefore, the properties of highly fractionated granite are of great significance for revealing the mineralization process of rare metal deposits.

The Ganfang intrusive suite, situated in the TBMD of the eastern Jiangnan Orogen (Fig. 1a), represents a significant component of the lithium mineralization-related granites in South China and comprises the Ganfang, Guyangzhai, Wutang, and Baishuidong plutons (Lou et al. 2023). Existing studies on these plutons focused on geology, geochronology, and whole-rock and isotopic geochemistry to examine their petrogenesis and links to lithium enrichment (Wang et al. 2017; Xie et al. 2019; Li et al. 2020; Nie et al. 2022; Xu et al. 2023). The highly fractionated Ganfang and Guyangzhai plutons were emplaced at ca. 147–144 Ma and 147–146 Ma, respectively (Wang et al. 2017). They possibly originated from the same magma chamber but underwent distinct assimilation processes (Wang et al. 2017). The ore-related Baishuidong pluton was emplaced at ca. 144 Ma (Xie et al. 2019). It consists of highly fractionated S-type granites, which were formed through the partial melting of

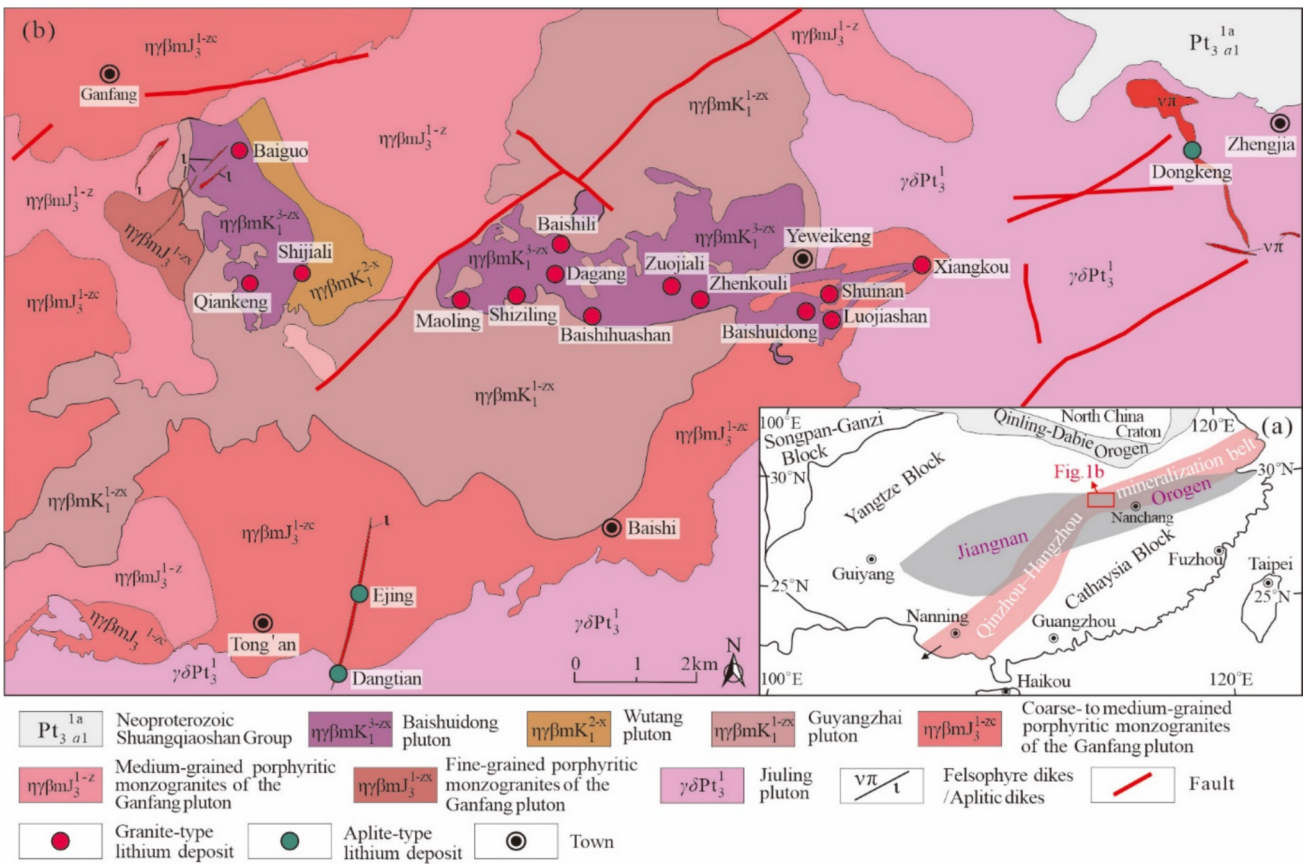


**Fig. 1** (**a**) Tectonic map of South China, showing the location of the Tong'an–Baishuidong lithium mining district (modified from Wang et al., 2017). (**b**) Regional geological map of the Tong'an–Baishuidong lithium mining district, showing the distribution of the major lithium deposits (modified from Zhang et al., 2021a; Lou et al., 2023)

metamorphosed pelites in an extensional setting (Li et al. 2020). By contrast, the nature and origin of the Wutang pluton remain unclear, limiting a comprehensive understanding of the entire Ganfang intrusive suite. In addition, the geodynamic setting of the granites in the district needs to be further revealed.

In this study, we present new monazite U–Pb dating, whole-rock geochemical, and Nd–Pb isotopic data for the Wutang granites to reveal their petrogenesis, magma source, and geodynamic setting. The new insights provide a scientific basis for an in-depth understanding of the Late Jurassic magmatism and its geodynamic setting in this district.

## 2 Regional geology

The Jiangnan Orogen strikes northeast and divides the South China Plate into the Yangtze Block and the Cathaysia Block (Fig. 1a; Wang et al. 2017). The TBMD lies in the eastern section of the Jiangnan Orogen (Fig. 1a). Currently, it comprises a dozen granite-related lithium deposits, such as the Qiankeng, Maoling, Dagang, and Baishihuashan deposits (Fig. 1b). The total $Li_2O$ reserves in the ores of these deposits exceed 1.659 million tons (Chen et al. 2023; Lou et al. 2023).

The exposed strata are primarily composed of the metamorphosed clastic sediments of the Anlelin Formation, which is part of the Neoproterozoic Shuangqiaoshan Group (Xu et al. 2014; Liu et al. 2023). Granitic magmatism occurred during the Neoproterozoic and again during the Jurassic-Cretaceous. A prominent example of the Neoproterozoic magmatism is the Jiuling pluton of the eastern TBMD (Fig. 1b). This pluton includes granodiorite, tonalite, and monzogranite, which were emplaced between 830 and 810 Ma (Duan et al. 2017; Rong 2017; Zhang et al. 2020). The regional-scale faults that strike E–W and N–E control the distribution of numerous Late Jurassic–Early Cretaceous granitic intrusions (Lou et al. 2023), mostly developed in the western part of the TBMD. The Late Jurassic–Early Cretaceous magmatism can be divided into four stages, which are represented by the Ganfang, Guyangzhai, Wutang, and Baishuidong plutons, respectively (Fig. 1b; Zhang et al. 2021a; Lou et al. 2023). These four plutons are collectively referred to as the Ganfang intrusive suite.

The ca. 153 $km^2$ Ganfang pluton is composed of coarse- to fine-grained porphyritic two-mica monzogranites, which have zircon U–Pb ages of $146.7 \pm 2.9$ Ma to $144.0 \pm 2.0$ Ma and were emplaced into the Jiuling pluton (Wang et al. 2017). The Guyangzhai pluton, with an exposed area exceeding 180 $km^2$, is composed of medium- to fine-grained porphyritic two-mica monzogranites. These rocks yield zircon U–Pb ages of $147.0 \pm 2.0$ Ma to $146.0 \pm 1.2$ Ma and were emplaced into the Jiuling and Ganfang plutons (Wang et al. 2017. Field and drill core observations indicate that the Wutang pluton is exposed in an area of ca. 24 $km^2$ and is composed of medium- to fine-grained two-mica monzogranites, intruding into the Ganfang and Guyangzhai plutons. The Baishuidong pluton crops out over an area of ca. 30 $km^2$ and consists of medium- to fine-grained muscovite granites, with a columbite U–Pb age of $144.0 \pm 5.0$ Ma (Xie et al. 2019; Lou et al. 2023). This pluton primarily intruded into the Wutang and Guyangzhai plutons, with a clear boundary of intrusion contact (Fig. 1b, 2a–c). In addition, these granitic plutons are cut by late-stage pegmatite, aplite, and porphyritic felsite dikes (Fig. 1b, 2a). The lithium ores usually occur in the upper part of the Baishuidong pluton, with lithium mainly enriched in muscovite, trilithionite, lepidolite, and small amounts of cookeite and amblygonite (Xie et al. 2019; Lou et al. 2023).

## 3 Samples and analytical methods

All Wutang granite samples analyzed in this study were collected from drill cores to avoid weathering and alteration. These granite samples range in color from gray-white to light red (Fig. 2d), containing 30%–35% alkali-feldspar, 25%–30% quartz, 20%–25% plagioclase, 5%–10% muscovite, and 5%–10% biotite (Fig. 2e–f). The alkali-feldspar and plagioclase are typically subhedral and range in diameter from 0.3 to 2.5 mm. The anhedral quartz grains have diameters of 0.2–2.0 mm, and they usually fill the gaps among the feldspars. The mica minerals are euhedral, with lengths ranging from 0.5 to 3.0 mm. The accessory minerals (< 1%) include apatite, zircon, monazite, cassiterite, and columbite.

The granite sample ZK2089-23 for monazite U–Pb dating was collected at a depth of 202.1 m of drill core ZK2809 in the Qiankeng mining area. Monazites were extracted via the heavy mineral separation technique, handpicked using a binocular microscope, pasted on a resin disk, and polished to exhibit their interior structures. These monazites occur as accessory minerals and feature euhedral-subhedral columnar and equiaxed shapes, with lengths and length/width ratios ranging from 40 to 130 μm and 1:1 to 2:1, respectively. Subsequently, back-scattered electron (BSE) images were taken to determine the placements for analysis. The above preparations were completed at Gaonianlinghang Technology Co., Ltd, Beijing. In situ monazite U–Pb isotopic analyses were performed at the State Key Laboratory of Nuclear Resources and Environment, East China University of Technology, using an Agilent 7900 ICP–MS equipped with a Coherent GeoLasHD 193-nm laser ablation system. The analyses were conducted using a beam diameter of 16 μm, an energy density of 3.5 J/$cm^2$, and an ablation frequency of 3 Hz. Helium served as the carrier gas of ablated material. As the make-up gas, argon was mixed with helium before entering

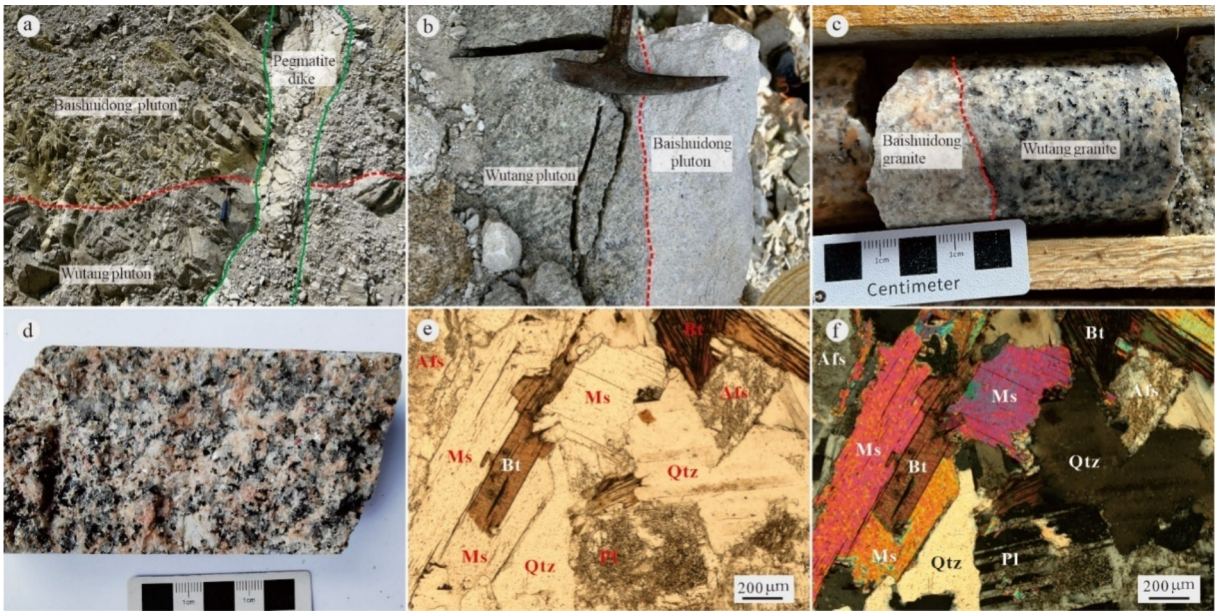


**Fig. 2** Field outcrops, hand specimen, and microscope images of the Wutang granites. (**a**) The Wutang pluton coexists closely with the Baishuidong pluton and is cut by the late-stage pegmatite dike. (**b–c**) The boundary between the Wutang and Baishuidong plutons. (**d**) Hand specimen of medium- to fine-grained two-mica monzogranites from the Wutang pluton. (**e-f**) Microscope images of medium- to fine-grained two-mica monzogranites from the Wutang pluton. Abbreviations: Afs = alkali-feldspar; Bt = biotite; Ms = muscovite; Pl = plagioclase; Qtz = quartz

the ICP to ensure steady and optimal excitation conditions. The monazite standards Bananeira and Diamantina were utilized to calibrate U–Pb isotopic fractionation and monitor data quality, respectively. The glass standard NIST-610 was utilized for trace element calibration. One Diamantina, one NIST-610, and two Bananeira standards were measured at the beginning and end of each set of eight unknown sample analyses. The weighted average $^{206}Pb/^{238}U$ ages of the Bananeira and Diamantina standards measured in this study were $513.7 \pm 11.0$ Ma and $497.9 \pm 3.9$ Ma, respectively, consistent with the reference $^{206}Pb/^{238}U$ ages of $513.6 \pm 1.2$ Ma for Bananeira and $495.3 \pm 0.5$ Ma for Diamantina (Goncalves et al. 2016, 2018). Each analysis comprised 20 s of background signal acquisition and 40 s of ablation signal acquisition. The masses measured in each ablation include $^{202}Hg$, $^{204}Pb$, $^{206}Pb$, $^{207}Pb$, $^{208}Pb$, $^{232}Th$, and $^{238}U$. The ICPMSDataCal software was used to process the raw isotopic data (Liu et al. 2010), and the ISOPLOT program was used to calculate the weighted mean age and draw the Concordia diagram (Ludwig 2003).

After detailed petrography observations, 14 Wutang granite samples from the Qiankeng and Dagang mining areas were selected for whole-rock geochemical analyses at the Nanchang Mineral Resources Supervision and Testing Center, Ministry of Land and Resources of China. The compositions of major and trace elements were measured using an x-ray fluorescence spectrometer (Axios-Max) and an ICP-MS (Agilent 7700x), respectively. The experimental precisions for major and trace elements are > 2% and 5%, respectively.

At the Wuhan Center of China Geological Survey, four whole-rock samples of the Wutang granite from the Qiankeng and Dagang mining areas were selected for Nd and Pb isotopic analyses. These granite samples were ground into powders of ca. 200 mesh and then digested with a mixture of $HClO_4$, $HNO_3$, and HF. The Sm and Nd concentrations and isotopic compositions were analyzed using a TRITON thermal ionization mass spectrometer. The measured Nd isotopic ratios are normalized to $^{146}Nd/^{144}Nd = 0.7219$. Standards GBW04419, GSW, and BCR-2 were used to monitor the stability and precision of instrumental analysis. Analyses of the BCR-2 standard demonstrate that the precision is > 1% for Sm and Nd concentrations and 0.5% for isotopic ratios. The measured average $^{143}Nd/^{144}Nd$ ratios of the GBW04419, GSW, and BCR-2 standards are $0.512712 \pm 0.000002$ (2σ), $0.512430 \pm 0.000005$ (2σ), and $0.512630 \pm 0.000008$ (2σ), respectively, consistent with the reference ratios of $0.512725 \pm 0.000007$ (2σ) for GBW04419, $0.512438 \pm 0.000006$ (2σ) for GSW, and 0.512618–0.512650 for BCR-2. Pb isotopic analyses were performed on a Neptune-Plus MC-ICP-MS, and the standard NBS981 was used for status monitoring of the instrument. Five analyses of NBS981 yield mean ratios of $^{206}Pb/^{204}Pb = 16.9417 \pm 0.0004$ (2σ), $^{207}Pb/^{204}Pb = 15.4984 \pm 0.0007$ (2σ), and

$^{208}Pb/^{204}Pb = 36.7195 \pm 0.0007$ (2σ), highly consistent with the recommended ratios of $^{206}Pb/^{204}Pb = 16.9405$, $^{207}Pb/^{204}Pb = 15.4963$, and $^{208}Pb/^{204}Pb = 36.7220$ (Galer and Abouchami 1998). The mass fractionation of Pb isotopic ratios was corrected by $^{203}Tl/^{205}Tl = 0.418652$, with an analysis precision $> \pm 0.05‰$.

## 4 Results

### 4.1 Monazite U–Pb dating

The U–Pb isotopic compositions of 23 monazite grains from sample ZK2089-23 are listed in Table 1. These monazite grains exhibit no apparent internal structure, indicating a homogeneous composition (Fig. 3a). The monazites have Th and U contents of 82,517–196,835 ppm and 895 to 22,236 ppm, respectively, with a wide Th/U ratio range of 40.2–168.0, indicating that they have a magmatic origin (Liang et al. 2022). In total, 23 spots were analyzed. The apparent $^{206}Pb/^{238}U$ ages vary from $140 \pm 4$ to $153 \pm 6$ Ma, yielding a weighted mean $^{206}Pb/^{238}U$ age of $145.8 \pm 1.0$ Ma (MSWD = 1.12; Fig. 3b), which is extremely consistent with the lower intercept age of $145.6 \pm 1.2$ Ma (MSWD = 1.15; Fig. 3a) and can be regarded as the intrusive age of the Wutang granites.

### 4.2 Major and trace elements

Table 2 shows the contents of major and trace elements of the Wutang granites. The $SiO_2$ and total alkali ($K_2O + Na_2O$) contents of the 14 Wutang granite samples are 72.80–73.40 wt% and 7.18–8.35 wt%, respectively, demonstrating silicon- and alkali-rich characteristics. In the $SiO_2 - (K_2O + Na_2O)$ diagram (Fig. 4a), the data for all samples are plotted within the field of granite. The granite samples have $K_2O$ contents and $K_2O/Na_2O$ ratios ranging from 4.71 wt% to 5.10 wt% and 1.5 to 2.5, respectively. In the $SiO_2 - K_2O$ diagram (Fig. 4b), all the data are plotted within the field of the high-K calc-alkaline series. The granite samples have A/CNK [molar $Al_2O_3/(CaO + K_2O + Na_2O)$] and A/NK ratios of 1.2–1.6 and 1.3–1.6, respectively, indicating that they are strongly peraluminous rocks (Fig. 4c). The corundum contents calculated by the CIPW standard mineral method range from 2.3 wt% to 5.5 wt%. In addition, the granite samples have a high differentiation index (DI = 90–92) and low MgO (0.27–0.43 wt%), CaO (0.44–0.90 wt%), $TiO_2$ (0.02–0.22 wt%), $P_2O_5$ (0.17–0.40 wt%), and TFeO (1.21–1.41 wt%) contents, implying that the granitic magma was highly fractionated.

In the primitive mantle-normalized trace element diagram (Fig. 5a), large-ion lithophile elements (LILEs) Rb and K, as well as HFSEs Th and U, are enriched, while LILEs Ba and Sr, as well as HFSEs Nb and Ti, are depleted. The total rare earth element (ΣREE) contents of the granite samples vary from 128 to 148 ppm. The contents of light rare earth elements (LREEs) and heavy rare earth elements (HREEs) are 119–138 ppm and 8.55–10.17 ppm, respectively, and the LREE/HREE ratios range from 13.3 to 15.2. The $(La/Yb)_N$ values range from 3.6–12.8, with an average of 7.5, showing a greater enrichment of LREEs. In the chondrite-normalized REE diagram (Fig. 5b), all the REE curves are inclined to the right, with apparent negative Eu anomalies ($\delta Eu = 0.3–0.4$).

### 4.3 Nd–Pb isotopic compositions

The whole-rock Nd–Pb isotopic data of the four Wutang granite samples are listed in Table 3. These samples contain 4.46–5.04 ppm of Sm and 22.21–24.83 ppm of Nd, and their $^{147}Sm/^{144}Nd$ and $^{143}Nd/^{144}Nd$ values range from 0.1172 to 0.1239 and 0.512175 to 0.512216, respectively. The εNd(t) values calculated based on the monazite U–Pb age (145.8 Ma; Fig. 3b) are between −9.0 and −8.2, corresponding to $T_{DM2}$ of 1488–1553 Ma. These granite samples have measured Pb isotopic ratios of $^{206}Pb/^{204}Pb = 18.56–18.86$, $^{207}Pb/^{204}Pb = 15.68–15.70$, and $^{208}Pb/^{204}Pb = 38.90–38.97$. Age corrections were conducted based on the age (145.8 Ma; Fig. 3b) and U, Th, and Pb concentrations of the granite samples (Table 2). The calculated initial Pb isotopic ratios are as follows: 18.38–18.55 for $(^{206}Pb/^{204}Pb)_i$, 15.67–15.68 for $(^{207}Pb/^{204}Pb)_i$, and 38.62–38.67 for $(^{208}Pb/^{204}Pb)_i$ (Table 3).

## 5 Discussion

### 5.1 The timing of the Wutang pluton

Wang et al. (2017) reported zircon U–Pb ages for the Guyangzhai pluton ranging from $147.0 \pm 2.0$ to $146.0 \pm 1.2$ Ma. Xie et al. (2019) reported a columbite U–Pb age of $144.0 \pm 5.0$ Ma for the Baishuidong pluton. In this study, we obtained a monazite U–Pb age of $145.8 \pm 1.0$ Ma for the Wutang pluton (Fig. 3b). Considering the error ranges, these intrusive ages are indistinguishable from one another. Nevertheless, field geological observations show that the Wutang pluton intruded the Guyangzhai pluton and was itself intruded by the Baishuidong pluton (Fig. 1b, 2a–c; Wang et al. 2017; Xu et al. 2024). Based on the aforementioned geological phenomena and chronological data, it can be inferred that the Wutang pluton was emplaced at the end of the Late Jurassic, with an intrusive age intermediate between those of the Guyangzhai and Baishuidong plutons.

**Table 1** LA-ICP-MS monazite U–Pb dating data of the Wutang granite (ZK2089-23)

| Sample spot | Th (ppm) | U (ppm) | Th/U | Isotopic ratios | | | | | |
|---|---|---|---|---|---|---|---|---|---|
| | | | | $^{207}Pb/^{206}Pb$ | 2σ | $^{207}Pb/^{235}U$ | 2σ | $^{206}Pb/^{238}U$ | 2σ |
| 01 | 186082 | 1108 | 168.0 | 0.0662 | 0.0126 | 0.2202 | 0.0332 | 0.0229 | 0.0012 |
| 02 | 167724 | 4572 | 36.7 | 0.0525 | 0.0048 | 0.1637 | 0.0140 | 0.0230 | 0.0008 |
| 03 | 177853 | 3351 | 53.1 | 0.0496 | 0.0053 | 0.1524 | 0.0156 | 0.0226 | 0.0008 |
| 04 | 174922 | 2371 | 73.8 | 0.0573 | 0.0071 | 0.1771 | 0.0202 | 0.0228 | 0.0008 |
| 05 | 82,517 | 12444 | 6.6 | 0.0507 | 0.0036 | 0.1590 | 0.0110 | 0.0228 | 0.0008 |
| 06 | 170347 | 4843 | 35.2 | 0.0537 | 0.0047 | 0.1676 | 0.0156 | 0.0224 | 0.0007 |
| 07 | 150489 | 18982 | 7.9 | 0.0524 | 0.0034 | 0.1636 | 0.0107 | 0.0225 | 0.0006 |
| 08 | 175230 | 4383 | 40.0 | 0.0550 | 0.0050 | 0.1718 | 0.0143 | 0.0230 | 0.0008 |
| 09 | 178082 | 895 | 199.1 | 0.0570 | 0.0110 | 0.2071 | 0.0339 | 0.0229 | 0.0013 |
| 10 | 180880 | 2059 | 87.8 | 0.0544 | 0.0069 | 0.1723 | 0.0196 | 0.0230 | 0.0009 |
| 11 | 181315 | 2544 | 71.3 | 0.0465 | 0.0057 | 0.1475 | 0.0175 | 0.0232 | 0.0008 |
| 12 | 163960 | 22236 | 7.4 | 0.0481 | 0.0025 | 0.1459 | 0.0076 | 0.0219 | 0.0006 |
| 13 | 125251 | 8792 | 14.3 | 0.0500 | 0.0034 | 0.1569 | 0.0105 | 0.0227 | 0.0007 |
| 14 | 156592 | 4092 | 38.3 | 0.0697 | 0.0061 | 0.2239 | 0.0202 | 0.0232 | 0.0008 |
| 15 | 189332 | 1152 | 164.4 | 0.0656 | 0.0096 | 0.2169 | 0.0301 | 0.0232 | 0.0009 |
| 16 | 185125 | 5383 | 34.4 | 0.0503 | 0.0042 | 0.1564 | 0.0128 | 0.0226 | 0.0008 |
| 17 | 139597 | 5872 | 23.8 | 0.0514 | 0.0045 | 0.1652 | 0.0152 | 0.0233 | 0.0008 |
| 18 | 196835 | 6849 | 28.7 | 0.0519 | 0.0035 | 0.1639 | 0.0105 | 0.0230 | 0.0008 |
| 19 | 173422 | 3256 | 53.3 | 0.0545 | 0.0061 | 0.1696 | 0.0175 | 0.0229 | 0.0008 |
| 20 | 176427 | 2399 | 73.6 | 0.0507 | 0.0071 | 0.1637 | 0.0196 | 0.0233 | 0.0008 |
| 21 | 177947 | 2189 | 81.3 | 0.0508 | 0.0058 | 0.1583 | 0.0164 | 0.0230 | 0.0008 |
| 22 | 179897 | 2171 | 82.9 | 0.0500 | 0.0056 | 0.1663 | 0.0194 | 0.0240 | 0.0009 |
| 23 | 170954 | 4252 | 40.2 | 0.0473 | 0.0047 | 0.1506 | 0.0143 | 0.0232 | 0.0008 |

| Sample spot | Apparent age (Ma) | | | | | |
|---|---|---|---|---|---|---|
| | $^{207}Pb/^{206}Pb$ | 2σ | $^{207}Pb/^{235}U$ | 2σ | $^{206}Pb/^{238}U$ | 2σ |
| 01 | 813 | 407 | 202 | 28 | 146 | 8 |
| 02 | 306 | 209 | 154 | 12 | 147 | 5 |
| 03 | 176 | 230 | 144 | 14 | 144 | 5 |
| 04 | 502 | 271 | 166 | 17 | 145 | 5 |
| 05 | 228 | 165 | 150 | 10 | 146 | 5 |
| 06 | 361 | 198 | 157 | 14 | 143 | 5 |
| 07 | 306 | 146 | 154 | 9 | 144 | 4 |
| 08 | 413 | 208 | 161 | 12 | 146 | 5 |
| 09 | 494 | 378 | 191 | 29 | 146 | 8 |
| 10 | 387 | 285 | 161 | 17 | 147 | 6 |
| 11 | 33 | 261 | 140 | 15 | 148 | 5 |
| 12 | 106 | 115 | 138 | 7 | 140 | 4 |
| 13 | 195 | 159 | 148 | 9 | 145 | 4 |
| 14 | 920 | 186 | 205 | 17 | 148 | 5 |
| 15 | 794 | 310 | 199 | 25 | 148 | 6 |
| 16 | 209 | -5 | 148 | 11 | 144 | 5 |
| 17 | 261 | 204 | 155 | 13 | 148 | 5 |
| 18 | 283 | 156 | 154 | 9 | 147 | 5 |
| 19 | 391 | 256 | 159 | 15 | 146 | 5 |
| 20 | 233 | 287 | 154 | 17 | 148 | 5 |
| 21 | 232 | 241 | 149 | 14 | 146 | 5 |
| 22 | 195 | 237 | 156 | 17 | 153 | 6 |

**Table 1** (continued)

| Sample spot | Apparent age (Ma) | | | | | |
|---|---|---|---|---|---|---|
| | $^{207}Pb/^{206}Pb$ | 2σ | $^{207}Pb/^{235}U$ | 2σ | $^{206}Pb/^{238}U$ | 2σ |
| 23 | 65 | 222 | 142 | 13 | 148 | 5 |

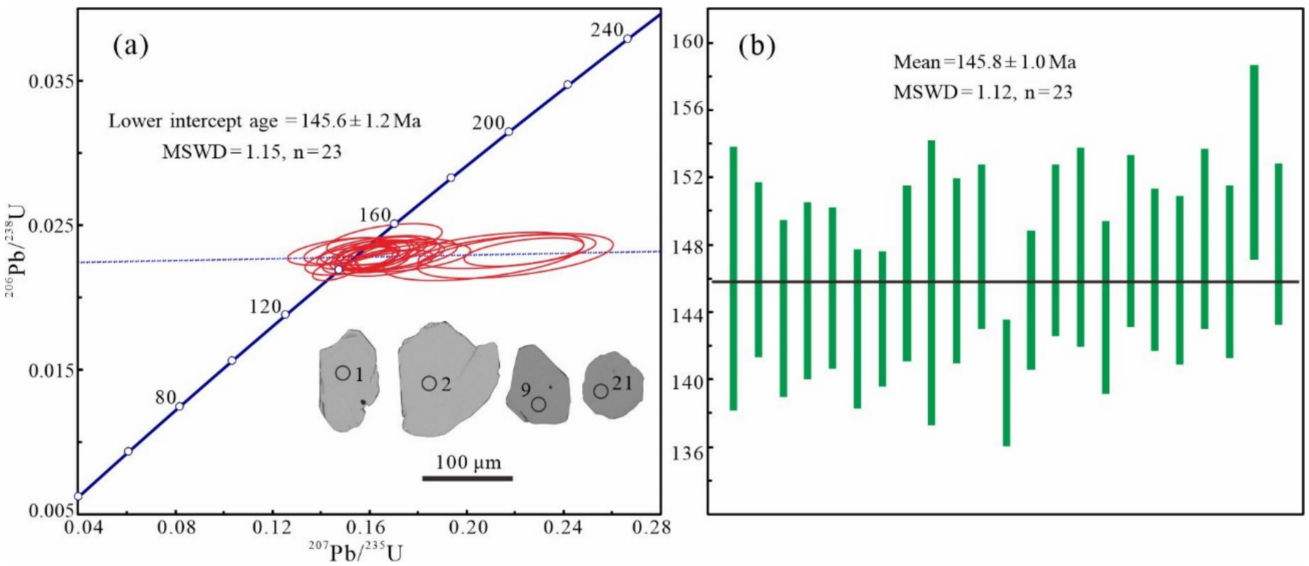


**Fig. 3** (**a**) Concordia diagrams of monazite U–Pb age for the Wutang granites, with BSE images of representative analyzed monazites. (**b**) The weighted mean 206Pb/238U age of monazite U–Pb dating for the Wutang granites

### 5.2 Petrogenesis

Previous studies have proposed that typical highly fractionated granites are geochemically distinguished by high contents of $SiO_2$ (> 72 wt%), low contents of CaO (< 1 wt%) and $MgO + TiO_2 + TFeO$ (< 6 wt%), high aluminum saturation indexes (peraluminous, A/CNK > 1.1) and differentiation indexes (DI > 88), low ratios of Nb/Ta (< 17) and Zr/Hf (< 38), and negative Eu anomalies (Bau 1996; Ballouard et al. 2016; Wu et al. 2017; Yang 2019). By contrast, the Wutang granites have high contents of $SiO_2$ (72.80–73.40 wt%), low contents of CaO (0.44–0.90 wt%) and $MgO + TiO_2 + TFeO$ (1.79–2.05 wt%), and high aluminum saturation indexes (A/CNK = 1.2–1.6) and differentiation indexes (DI = 90–92) (Table 1), indicating highly fractionated characteristics. The negative Eu anomalies ($\delta$Eu = 0.3–0.4) and relative depletion of Sr, Ti, and Nb may be attributed to the fractional crystallization of minerals such as plagioclase, apatite, ilmenite, rutile, and titanite during magma evolution (Zhang et al. 2021b; Xu et al. 2022; Yang et al. 2023). Furthermore, these granites exhibit negative Eu anomalies ($\delta$Eu = 0.3–0.4), high Rb contents (373–467 ppm) and Rb/Sr ratios (4.7–8.1), moderate Ba contents (239–278 ppm), as well as low Sr contents (52.7–82.0 ppm) and Nb/Ta (2.2–5.3) and Zr/Hf (21.3–31.5) ratios, all of which indicate that they are highly fractionated (Zaraisky et al. 2009; Ballouard et al. 2016). In the $(K_2O + Na_2O)/CaO - (Zr + Nb + Ce + Y)$ diagram (Fig. 6a), the samples are plotted in the fractionated granite field. In the Rb−Ba−Sr diagram (Fig. 6b), the samples are projected into the field of highly fractionated granite. Collectively, the above geochemical features reveal that the Wutang granites are highly fractionated.

Granites are typically classified as I-, S-, M-, or A-type based on the discrepancies in chemical composition, magma origin, and geodynamic setting (e.g., Collins et al. 1982; Whalen 1985; Whalen et al. 1987; Chappell 1999; Chappell and White 2001; Wu et al. 2007; Rong 2017). However, highly fractionated granites, regardless of type, have mineral and chemical compositions that are analogous to eutectic granites. As a result, the type of highly fractionated granites needs to be comprehensively determined based on their petrographic and geochemical features (Wu et al. 2015; Lan et al. 2020). In addition, the M-type granites are rare in the continental crust, often plagioclase granites that coexist with ophiolites (Rong 2017; Hu et al. 2023). This is notably different from the lithology and formation environment of the Wutang granites. Thus,

**Table 2** Data of the major elements (wt%) and trace elements (ppm) in the Wutang granites

| Sample no | ZK2802-10 | ZK2802-20 | ZK0001-1 | ZK2809-1 | ZK2809-4 | ZK2809-5 | ZK2809-6 |
|---|---|---|---|---|---|---|---|
| $SiO_2$ | 73.11 | 72.99 | 73.14 | 72.88 | 73.40 | 72.89 | 73.34 |
| $Al_2O_3$ | 14.60 | 14.70 | 14.50 | 14.79 | 14.24 | 14.72 | 14.40 |
| $TiO_2$ | 0.22 | 0.22 | 0.20 | 0.21 | 0.20 | 0.21 | 0.21 |
| TFeO | 1.39 | 1.36 | 1.30 | 1.37 | 1.32 | 1.37 | 1.37 |
| CaO | 0.44 | 0.81 | 0.66 | 0.80 | 0.88 | 0.90 | 0.60 |
| MgO | 0.39 | 0.40 | 0.38 | 0.39 | 0.27 | 0.37 | 0.37 |
| $K_2O$ | 5.10 | 4.98 | 4.71 | 5.10 | 4.96 | 4.96 | 4.92 |
| $Na_2O$ | 2.08 | 3.23 | 3.22 | 3.22 | 3.30 | 3.32 | 3.05 |
| MnO | 0.04 | 0.04 | 0.04 | 0.04 | 0.04 | 0.03 | 0.04 |
| $P_2O_5$ | 0.22 | 0.19 | 0.40 | 0.20 | 0.19 | 0.20 | 0.20 |
| LOI | 2.19 | 0.86 | 1.25 | 0.78 | 0.88 | 0.82 | 1.29 |
| Total | 99.82 | 99.80 | 99.80 | 99.80 | 99.70 | 99.81 | 99.82 |
| $Na_2O+K_2O$ | 7.18 | 8.21 | 7.93 | 8.32 | 8.26 | 8.28 | 7.97 |
| $K_2O/Na_2O$ | 2.5 | 1.5 | 1.5 | 1.6 | 1.5 | 1.5 | 1.6 |
| $CaO/Na_2O$ | 0.21 | 0.25 | 0.20 | 0.25 | 0.27 | 0.27 | 0.20 |
| A/CNK | 1.6 | 1.3 | 1.4 | 1.3 | 1.2 | 1.2 | 1.3 |
| A/NK | 1.6 | 1.4 | 1.4 | 1.4 | 1.3 | 1.4 | 1.4 |
| $Mg^{\#}$ | 33.6 | 34.6 | 34.5 | 33.9 | 26.9 | 32.7 | 32.7 |
| DI | 90 | 90 | 91 | 90 | 91 | 90 | 91 |
| La | 27.00 | 28.00 | 26.40 | 27.40 | 26.90 | 26.50 | 24.60 |
| Ce | 64.4 | 64.9 | 63.2 | 66.3 | 65 | 63.3 | 58.3 |
| Pr | 6.88 | 7.09 | 6.74 | 6.99 | 6.84 | 6.74 | 6.24 |
| Nd | 26.90 | 27.70 | 26.20 | 26.90 | 26.60 | 25.90 | 24.50 |
| Sm | 5.16 | 5.25 | 5.21 | 5.30 | 5.22 | 5.15 | 4.74 |
| Eu | 0.61 | 0.66 | 0.57 | 0.63 | 0.61 | 0.59 | 0.59 |
| Gd | 4.54 | 4.70 | 4.45 | 4.70 | 4.46 | 4.39 | 4.04 |
| Tb | 0.51 | 0.53 | 0.49 | 0.51 | 0.51 | 0.52 | 0.47 |
| Dy | 2.16 | 2.29 | 2.08 | 2.19 | 2.28 | 2.33 | 2.06 |
| Ho | 0.37 | 0.39 | 0.35 | 0.37 | 0.38 | 0.40 | 0.35 |
| Er | 0.87 | 0.92 | 0.83 | 0.87 | 0.91 | 0.98 | 0.86 |
| Tm | 0.11 | 0.12 | 0.11 | 0.12 | 0.12 | 0.12 | 0.11 |
| Yb | 0.65 | 0.71 | 0.62 | 0.67 | 0.70 | 0.74 | 0.69 |
| Lu | 0.10 | 0.10 | 0.10 | 0.11 | 0.10 | 0.11 | 0.10 |
| Y | 10.10 | 10.50 | 9.63 | 10.10 | 10.60 | 11.20 | 9.78 |
| Cu | 3.11 | 3.15 | 4.65 | 4.59 | 7.79 | 6.73 | 5.32 |
| Pb | 33.10 | 40.10 | 42.00 | 42.70 | 39.90 | 40.90 | 40.20 |
| Zn | 66.1 | 61.1 | 60.4 | 69.4 | 65.0 | 67.9 | 68.3 |
| Cr | 6.24 | 6.96 | 8.60 | 6.76 | 6.57 | 7.82 | 5.96 |
| Ni | 1.76 | 1.64 | 1.57 | 2.40 | 1.85 | 1.77 | 2.02 |
| Co | 2.63 | 2.57 | 3.09 | 2.86 | 2.38 | 2.50 | 2.52 |
| Li | 298 | 224 | 302 | 251 | 260 | 204 | 269 |
| Rb | 409 | 373 | 440 | 386 | 382 | 380 | 388 |
| Cs | 100.0 | 80.5 | 99.6 | 73.9 | 87.6 | 65.7 | 65.4 |
| W | 10.00 | 3.37 | 5.50 | 3.68 | 14.30 | 2.12 | 6.87 |
| Mo | 0.12 | 0.16 | 0.18 | 0.22 | 0.33 | 0.19 | 0.16 |
| Sr | 52.7 | 75.4 | 54.6 | 82.0 | 77.4 | 76.7 | 66.6 |
| Ba | 252 | 265 | 242 | 265 | 255 | 266 | 263 |
| V | 26.20 | 25.60 | 25.30 | 25.80 | 25.40 | 24.70 | 26.30 |
| Sc | 3.24 | 3.19 | 3.25 | 3.40 | 3.22 | 3.16 | 3.12 |
| Nb | 12.30 | 16.60 | 13.00 | 13.40 | 14.00 | 12.40 | 12.50 |

**Table 2** (continued)

| Sample no | ZK2802-10 | ZK2802-20 | ZK0001-1 | ZK2809-1 | ZK2809-4 | ZK2809-5 | ZK2809-6 |
|---|---|---|---|---|---|---|---|
| Ta | 2.50 | 3.56 | 3.33 | 3.44 | 3.30 | 2.77 | 2.54 |
| Zr | 112.90 | 109.40 | 101.70 | 106.20 | 106.80 | 104.50 | 106.40 |
| Hf | 3.58 | 5.13 | 4.76 | 4.55 | 4.24 | 4.20 | 4.12 |
| Be | 10.10 | 13.20 | 17.00 | 10.50 | 13.00 | 9.00 | 10.30 |
| Ga | 23.20 | 23.10 | 22.20 | 23.20 | 23.00 | 23.20 | 24.00 |
| Sn | 18.30 | 16.30 | 30.40 | 21.90 | 22.50 | 17.50 | 17.80 |
| Tl | 2.09 | 1.86 | 2.54 | 2.02 | 2.05 | 1.91 | 1.95 |
| U | 5.44 | 5.56 | 5.22 | 9.27 | 11.20 | 4.62 | 5.03 |
| Th | 23.00 | 23.40 | 22.30 | 22.60 | 23.20 | 22.20 | 20.70 |
| LREE | 131 | 134 | 128 | 134 | 131 | 128 | 119 |
| HREE | 9.31 | 9.76 | 9.02 | 9.54 | 9.46 | 9.58 | 8.68 |
| ΣREE | 140 | 143 | 137 | 143 | 141 | 138 | 128 |
| LREE/HREE | 14.1 | 13.7 | 14.2 | 14.0 | 13.9 | 13.4 | 13.7 |
| $\delta$Eu | 0.38 | 0.4 | 0.35 | 0.38 | 0.38 | 0.37 | 0.4 |
| $(La/Yb)_N$ | 29.9 | 28.4 | 30.5 | 29.3 | 27.6 | 25.7 | 25.6 |
| $(La/Sm)_N$ | 3.4 | 3.4 | 3.3 | 3.3 | 3.3 | 3.3 | 3.4 |
| $(Gd/Yb)_N$ | 5.8 | 5.5 | 5.9 | 5.8 | 5.3 | 4.9 | 4.9 |
| Zr+Nb+Ce+Y | 200 | 201 | 188 | 196 | 196 | 191 | 187 |
| Rb/Sr | 7.8 | 5.0 | 8.1 | 4.7 | 4.9 | 5.0 | 5.8 |
| Zr/Hf | 31.5 | 21.3 | 21.4 | 23.3 | 25.2 | 24.9 | 25.8 |
| Nb/Ta | 4.9 | 2.2 | 3.9 | 3.9 | 4.2 | 4.5 | 4.9 |
| Corundum | 5.5 | 3.0 | 3.9 | 3.0 | 2.3 | 2.7 | 3.5 |

| Sample no | ZK2809-20 | ZK2809-22 | ZK2809-23 | ZKSHK1-6 | ZKSHK2-1 | ZK2001-1 | ZK3209-2 |
|---|---|---|---|---|---|---|---|
| $SiO_2$ | 73.04 | 72.84 | 72.80 | 73.34 | 72.94 | 73.29 | 73.16 |
| $Al_2O_3$ | 14.66 | 14.66 | 14.70 | 14.32 | 14.65 | 14.39 | 14.70 |
| $TiO_2$ | 0.21 | 0.21 | 0.21 | 0.20 | 0.22 | 0.22 | 0.20 |
| TFeO | 1.40 | 1.34 | 1.38 | 1.27 | 1.41 | 1.33 | 1.21 |
| CaO | 0.50 | 0.84 | 0.90 | 0.65 | 0.78 | 0.71 | 0.66 |
| MgO | 0.43 | 0.41 | 0.43 | 0.33 | 0.42 | 0.28 | 0.39 |
| $K_2O$ | 4.97 | 4.94 | 5.00 | 4.87 | 4.96 | 4.98 | 4.79 |
| $Na_2O$ | 3.08 | 3.16 | 3.15 | 3.29 | 3.20 | 3.37 | 3.24 |
| MnO | 0.04 | 0.04 | 0.04 | 0.06 | 0.04 | 0.06 | 0.06 |
| $P_2O_5$ | 0.19 | 0.19 | 0.19 | 0.33 | 0.21 | 0.25 | 0.17 |
| LOI | 1.24 | 1.04 | 0.96 | 1.15 | 0.95 | 0.90 | 1.10 |
| Total | 99.79 | 99.68 | 99.78 | 99.89 | 99.81 | 99.80 | 99.70 |
| $Na_2O+K_2O$ | 8.05 | 8.10 | 8.15 | 8.16 | 8.16 | 8.35 | 8.03 |
| $K_2O/Na_2O$ | 1.6 | 1.6 | 1.6 | 1.5 | 1.6 | 1.5 | 1.5 |
| $CaO/Na_2O$ | 0.16 | 0.27 | 0.29 | 0.20 | 0.24 | 0.21 | 0.20 |
| A/CNK | 1.3 | 1.3 | 1.3 | 1.3 | 1.3 | 1.2 | 1.3 |
| A/NK | 1.4 | 1.4 | 1.4 | 1.3 | 1.4 | 1.3 | 1.4 |
| $Mg^{\#}$ | 35.5 | 35.6 | 35.9 | 31.8 | 34.9 | 27.5 | 36.7 |
| DI | 91 | 90 | 90 | 92 | 90 | 92 | 91 |
| La | 27.30 | 27.70 | 28.70 | 25.50 | 28.00 | 26.80 | 26.60 |
| Ce | 66.2 | 68.3 | 67.9 | 61.1 | 65.1 | 63.4 | 64.5 |
| Pr | 6.95 | 7.10 | 7.23 | 6.60 | 6.97 | 6.97 | 6.78 |
| Nd | 27.20 | 28.00 | 28.20 | 25.50 | 27.00 | 27.10 | 26.30 |
| Sm | 5.32 | 5.32 | 5.52 | 5.03 | 4.97 | 5.13 | 5.09 |
| Eu | 0.56 | 0.60 | 0.59 | 0.59 | 0.62 | 0.56 | 0.50 |
| Gd | 4.52 | 4.45 | 4.74 | 4.31 | 4.43 | 4.21 | 4.28 |

**Table 2** (continued)

| Sample no | ZK2809-20 | ZK2809-22 | ZK2809-23 | ZKSHK1-6 | ZKSHK2-1 | ZK2001-1 | ZK3209-2 |
|---|---|---|---|---|---|---|---|
| Tb | 0.51 | 0.52 | 0.55 | 0.50 | 0.49 | 0.45 | 0.47 |
| Dy | 2.25 | 2.35 | 2.46 | 2.24 | 2.16 | 1.99 | 2.09 |
| Ho | 0.39 | 0.40 | 0.43 | 0.39 | 0.38 | 0.34 | 0.36 |
| Er | 0.89 | 0.94 | 1.02 | 0.94 | 0.87 | 0.76 | 0.85 |
| Tm | 0.11 | 0.12 | 0.13 | 0.12 | 0.12 | 0.11 | 0.11 |
| Yb | 0.67 | 0.71 | 0.74 | 0.73 | 0.69 | 0.62 | 0.68 |
| Lu | 0.10 | 0.11 | 0.11 | 0.10 | 0.10 | 0.09 | 0.10 |
| Y | 10.70 | 11.20 | 11.80 | 10.80 | 10.20 | 9.04 | 9.96 |
| Cu | 0.26 | 4.42 | 18.70 | 6.03 | 11.40 | 2.58 | 5.32 |
| Pb | 38.20 | 42.20 | 39.40 | 40.00 | 37.40 | 38.30 | 42.00 |
| Zn | 65.3 | 67.7 | 66.0 | 62.6 | 61.4 | 76.4 | 66.9 |
| Cr | 5.58 | 7.30 | 6.94 | 4.73 | 8.67 | 4.88 | 7.44 |
| Ni | 1.73 | 1.49 | 1.69 | 1.44 | 1.93 | 1.22 | 1.96 |
| Co | 2.60 | 2.62 | 2.62 | 2.36 | 2.73 | 2.34 | 2.38 |
| Li | 303 | 264 | 254 | 207 | 268 | 295 | 448 |
| Rb | 384 | 377 | 380 | 377 | 422 | 459 | 467 |
| Cs | 63.9 | 72.0 | 68.3 | 54.9 | 107.0 | 87.7 | 113.4 |
| W | 6.18 | 3.91 | 8.35 | 5.04 | 11.70 | 5.33 | 4.12 |
| Mo | 0.16 | 1.57 | 0.24 | 0.13 | 0.20 | 0.12 | 0.14 |
| Sr | 66.0 | 68.5 | 74.4 | 65.6 | 70.9 | 67.2 | 62.9 |
| Ba | 259 | 261 | 257 | 239 | 278 | 244 | 245 |
| V | 24.50 | 25.00 | 26.60 | 23.60 | 24.70 | 24.70 | 25.90 |
| Sc | 3.26 | 3.40 | 3.36 | 3.15 | 3.51 | 2.68 | 2.99 |
| Nb | 12.20 | 12.40 | 12.10 | 12.60 | 12.80 | 13.80 | 13.50 |
| Ta | 2.32 | 2.46 | 2.32 | 2.85 | 3.03 | 3.85 | 3.52 |
| Zr | 106.20 | 109.20 | 107.40 | 97.80 | 113.70 | 109.80 | 100.90 |
| Hf | 4.04 | 4.56 | 4.21 | 4.49 | 5.28 | 4.69 | 3.82 |
| Be | 12.70 | 12.50 | 12.50 | 15.20 | 9.33 | 12.10 | 21.70 |
| Ga | 23.00 | 23.10 | 23.50 | 22.00 | 24.00 | 23.70 | 23.20 |
| Sn | 14.00 | 17.60 | 15.60 | 18.40 | 20.20 | 20.30 | 23.20 |
| Tl | 1.89 | 1.95 | 1.86 | 1.84 | 2.15 | 2.36 | 2.46 |
| U | 8.43 | 7.70 | 8.29 | 5.59 | 6.26 | 4.19 | 8.25 |
| Th | 23.60 | 23.80 | 24.10 | 21.40 | 23.70 | 23.50 | 23.20 |
| LREE | 134 | 137 | 138 | 124 | 133 | 130 | 130 |
| HREE | 9.45 | 9.59 | 10.17 | 9.34 | 9.24 | 8.55 | 8.95 |
| ΣREE | 143 | 147 | 148 | 134 | 142 | 139 | 139 |
| LREE/HREE | 14.1 | 14.3 | 13.6 | 13.3 | 14.4 | 15.2 | 14.5 |
| $\delta$Eu | 0.34 | 0.37 | 0.35 | 0.38 | 0.4 | 0.35 | 0.32 |
| $(La/Yb)_N$ | 29.1 | 28.0 | 28.0 | 25.1 | 29.2 | 31.3 | 28.2 |
| $(La/Sm)_N$ | 3.3 | 3.4 | 3.4 | 3.3 | 3.6 | 3.4 | 3.4 |
| $(Gd/Yb)_N$ | 5.6 | 5.2 | 5.3 | 4.9 | 5.3 | 5.7 | 5.2 |
| Zr + Nb + Ce + Y | 195 | 201 | 199 | 182 | 202 | 196 | 189 |
| Rb/Sr | 5.8 | 5.5 | 5.1 | 5.8 | 6.0 | 6.8 | 7.4 |
| Zr/Hf | 26.3 | 24.0 | 25.5 | 21.8 | 21.5 | 23.4 | 26.4 |
| Nb/Ta | 5.3 | 5.0 | 5.2 | 4.4 | 4.2 | 3.6 | 3.8 |
| Corundum | 3.8 | 3.1 | 2.9 | 3.3 | 3.1 | 2.8 | 3.4 |

TFeO = FeO + ($Fe_2O_3$ × 0.8998); LOI = loss on ignition; A/CNK = molar [$Al_2O_3$/(CaO + $Na_2O$ + $K_2O$)]; A/NK = molar [$Al_2O_3$/($Na_2O$ + $K_2O$)]; $Mg^{\#} = 100Mg^{2+}/(Mg^{2+} + TFe^{2+})$

$\delta Eu = 2w(Eu)_N/[w(Gd)_N + w(Sm)_N]$

The letter 'N' in the footnote stands for chondrite normalization, and the values referred to Sun and Mcdonough (1989)

DI, differentiation indexes; LREE, light rare earth element; HREE, heavy rare earth element; ΣREE, total rare earth elements

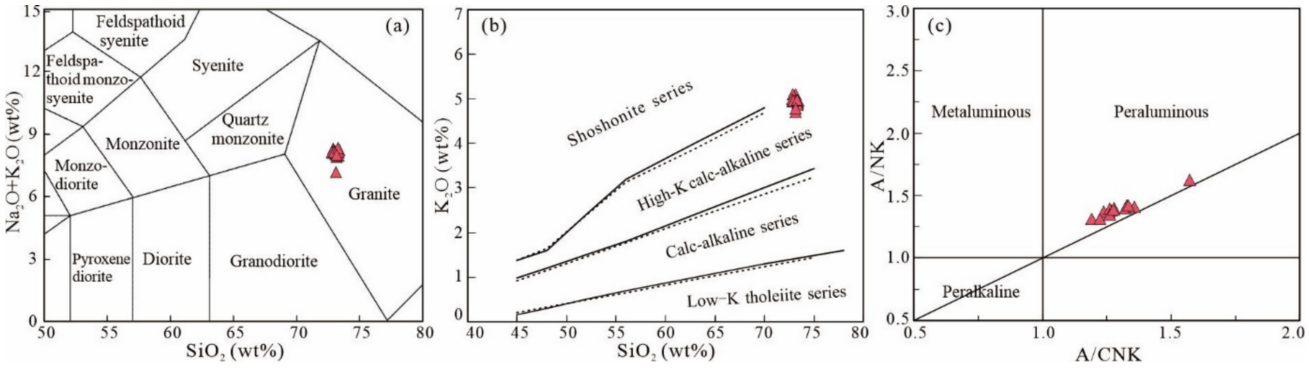


**Fig. 4** Geochemical diagrams of the Wutang granites. (**a**) $SiO_2$−($K_2O$+$Na_2O$) diagram (after Middlemost, 1994). (**b**) $SiO_2$−$K_2O$ diagram (after Peccerillo and Taylor, 1976). (**c**) A/CNK−A/NK diagram (after Maniar and Piccoli, 1989)

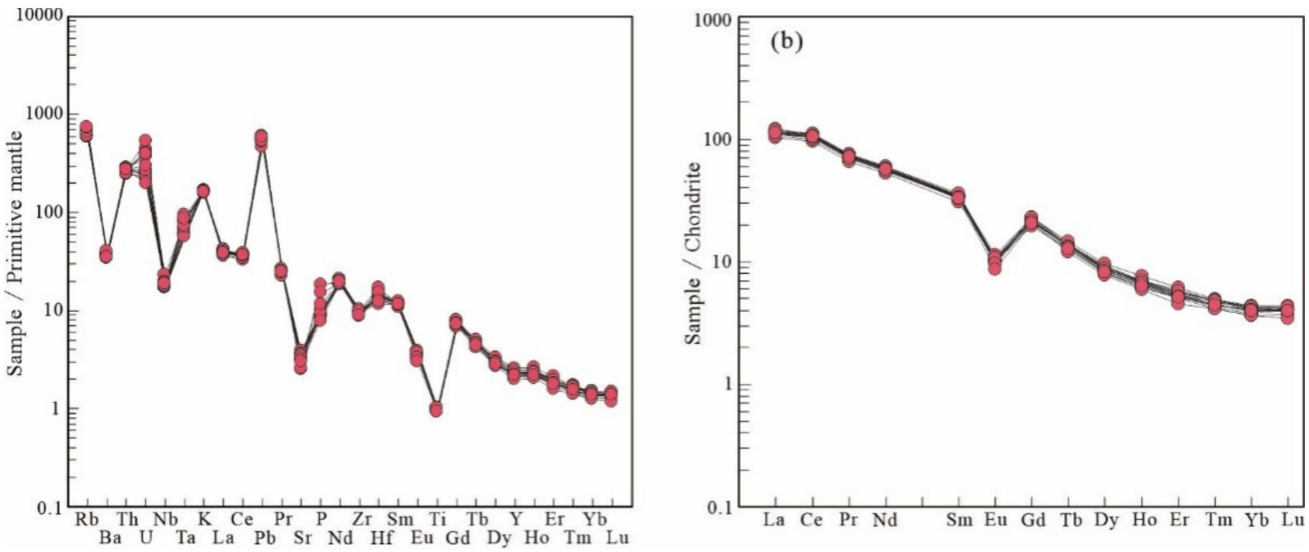


**Fig. 5** (**a**) Primitive mantle-normalized trace element spider-grams and (**b**) chondrite-normalized REE distribution patterns of the Wutang granites. Primitive-mantle and chondrite values are from Sun and McDonough (1989)

the possibility of M-type granites was not discussed in this study.

The Wutang granites have Zr+Nb+Ce+Y values ranging from 182 to 202 ppm, which are significantly lower than those of the A-type granites (350 ppm; Whalen et al. 1987). In the ($K_2O + Na_2O$)/CaO−(Zr + Nb + Ce + Y) diagram (Fig. 6a), all data are plotted outside the field of A-type granites. The calculated zircon saturation temperatures of the Wutang granites vary from 700 to 770 °C, which are substantially lower than those of the A-type granites (839–900 °C; Watson and Harrison 1983; King et al. 1997). Furthermore, the $SiO_2$−TFeO/MgO diagram (Fig. 6c) illustrates that the Wutang granites should be I- or S-type rather than A-type. Therefore, the possibility of A-type granites can be ruled out.

The petrographic observation indicates that the Wutang granites contain 5–10 wt% muscovite but no hornblende (Fig. 2e and f). The corundum contents calculated by the CIPW standard mineral method are between 2.3 wt% and 5.5 wt% (Table 2; Lu and Li 2021). These petrographic features are similar to those of the S-type granites instead of the I-type granites. The granites have high aluminum saturation indexes (A/CNK = 1.2−1.6). Hence, they are classified as strongly peraluminous rocks (Fig. 4c). In the discriminating diagrams of S- and I-type granites (Fig. 6d–f), all samples fall into the field of S-type granites. Additionally, the Th and Y contents of the Wutang granites are relatively low and have a slightly negative correlation with Rb, displaying an evolutionary trend of the S-type granites in the Rb−Th and Rb−Y diagrams (Fig. 6g and h; Chappell 1999). Based on the aforementioned petrographic and compositional features, the granites of the Wutang pluton are classified as highly fractionated S-type granites.

**Table 3** Whole-rock Nd-Pb isotopic data for the Wutang granites

| Sample No. | Nd isotopic composition | | | | | | Pb isotopic composition | | | | |
|---|---|---|---|---|---|---|---|---|---|---|---|
| | Sm/ppm | Nd/ppm | $^{147}Sm/^{144}Nd$ | $^{143}Nd/^{144}Nd$ | $\varepsilon_{Nd}(t)$ | $T_{DM2}$/Ma | $^{206}Pb/^{204}Pb$ | $^{207}Pb/^{204}Pb$ | $^{208}Pb/^{204}Pb$ | $(^{206}Pb/^{204}Pb)_i$ | $(^{207}Pb/^{204}Pb)_i$ | $(^{208}Pb/^{204}Pb)_i$ |
| ZK0001-1 | 4.46 | 22.21 | 0.1215 | 0.512179 | −9.0 | 1547 | 18.56 | 15.68 | 38.92 | 18.38 | 15.67 | 38.67 |
| ZK2809-1 | 5.02 | 24.64 | 0.1232 | 0.512216 | −8.2 | 1489 | 18.86 | 15.70 | 38.91 | 18.55 | 15.68 | 38.67 |
| ZK2809-23 | 5.04 | 24.61 | 0.1239 | 0.512179 | −9.0 | 1547 | 18.69 | 15.69 | 38.90 | 18.40 | 15.67 | 38.62 |
| ZKSHK2-1 | 4.81 | 24.83 | 0.1172 | 0.512175 | −9.0 | 1553 | 18.73 | 15.69 | 38.97 | 18.50 | 15.68 | 38.67 |

The letter 'i' in the footnote stands for initial Pb isotopic ratios

**Fig. 6** Discrimination diagrams of genetic type for the Wutang granites. (**a**) $[(K_2O+Na_2O)/CaO]-(Zr+Nb+Ce+Y)$ diagram (after Whalen et al., 1987). (**b**) Rb−Ba−Sr diagram (after Bouseily and Sokkary, 1975). (**c**) $SiO_2-(TFeO/MgO)$ diagram (after Whalen et al., 1987). (**d**) $SiO_2-Zr$ diagram (after Watson and Harrison, 1983). (**e**) Zr−TiO2 diagram (after Watson and Harrison, 1983). (**f**) A−C−F diagram (after Nakada and Takahashi, 1979). (**g**) Rb−Th diagram (after Chappell, 1999). (**h**) Rb−Y diagram (after Chappell, 1999). A = molar ($Al2O_3$ - $Na_2O$ - K2O), C= molar (CaO - 3.33P2O5), F = molar (FeO + MgO + MnO)

### 5.3 Magma source

The Wutang granites are strongly peraluminous granites (A/CNK = 1.2 − 1.6), which are typically considered a result of the partial melting of metasedimentary rocks (Koester et al. 2002; Lan et al. 2020). These granites have Rb/Sr ratios of 4.7−8.1 (average of 6.0) and Nb/Ta ratios of 2.2−5.3 (average of 4.3), which are closer to the standard ratios of crust-derived rocks than mantle-derived rocks [Rb/Sr ratios: 0.35 for crust and 0.034 for mantle (Rudnick and Fountain 1995; Taylor and Mclennan 1995); Nb/Ta ratios: 11−12 for crust and 17.5 for mantle (Green 1995)]. In the diagrams of $\delta Eu-(La/Yb)_N$ (Fig. 7a) and $\delta Eu-(Na_2O+K_2O)$(Fig. 7b), all samples are projected into the field of crust-derived granites. Their $\varepsilon_{Nd}(t)$ values and $T_{DM2}$ range from −9.03 to −8.23 and 1488 Ma to 1553 Ma, respectively. In the $t-\varepsilon_{Nd}(t)$ diagram (Fig. 8a), all samples fall within the field of the Proterozoic crustal basement rocks in South China, consistent with the $T_{DM2}$. Though no ages of inherited or captured monazites were obtained from the Wutang granites, the Ganfang and Guyangzhai granites contain some Neoproterozoic zircon cores (ca. 870−820 Ma), which were identified as captured zircons associated with the wall-rock assimilation process (Wang et al. 2017). These geochemical and geochronological features indicate that the Wutang granites primarily originated from the partial melting of ancient crustal materials and might have undergone wall-rock assimilation during magma migration. Moreover, the granite samples are plotted above the upper crust field and along the upper crust evolution line in the diagrams of Nb/Y−Th/Y (Fig. 7c) and $^{206}Pb/^{204}Pb-^{207}Pb/^{204}Pb$ (Fig. 8b), respectively, also demonstrating that the granitic magma was mainly derived from the remelting of crustal materials.

For strongly peraluminous granites with $SiO_2$ content ranging from 67 wt% to 77 wt%, the $CaO/Na_2O$ ratio can efficiently reflect the material composition of their magma source (Jian et al. 2018). More precisely, the peraluminous granites generated by the partial melting of psammites have $CaO/Na_2O$ ratios > 0.3, while those generated by the partial melting of pelites have $CaO/Na_2O$ ratios < 0.3 (Sylvester 1998). The $CaO/Na_2O$ ratios of the Wutang granites range from 0.16 to 0.29 (average of 0.23; Table 2), all of which are < 0.3, suggesting a pelite-rich source. In the Rb/Sr−Rb/

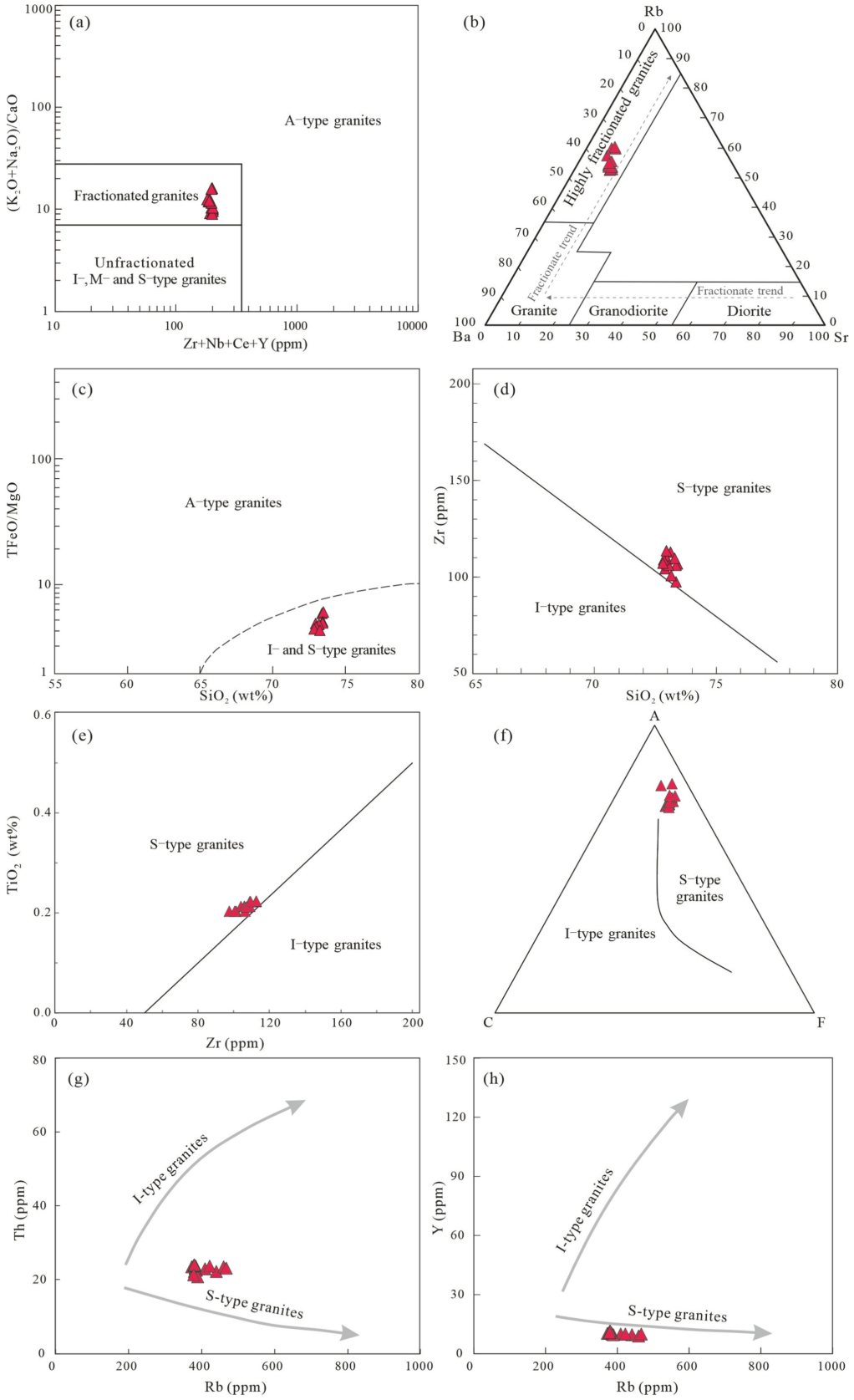
(a)
A–type granites
Fractionated granites
Unfractionated
I–,M– and S–type granites
(K2O+Na2O)/CaO
Zr+Nb+Ce+Y (ppm)
(b)
Rb
Ba
Sr
Highly fractionated granites
Fractionate trend
Fractionate trend
Granite
Granodiorite
Diorite
(c)
A–type granites
I– and S–type granites
TFeO/MgO
SiO2 (wt%)
(d)
S–type granites
I–type granites
Zr (ppm)
SiO2 (wt%)
(e)
S–type granites
I–type granites
TiO2 (wt%)
Zr (ppm)
(f)
A
S–type
granites
I–type granites
C
F
(g)
I-type granites
S-type granites
Th (ppm)
Rb (ppm)
(h)
I-type granites
S-type granites
Y (ppm)
Rb (ppm)

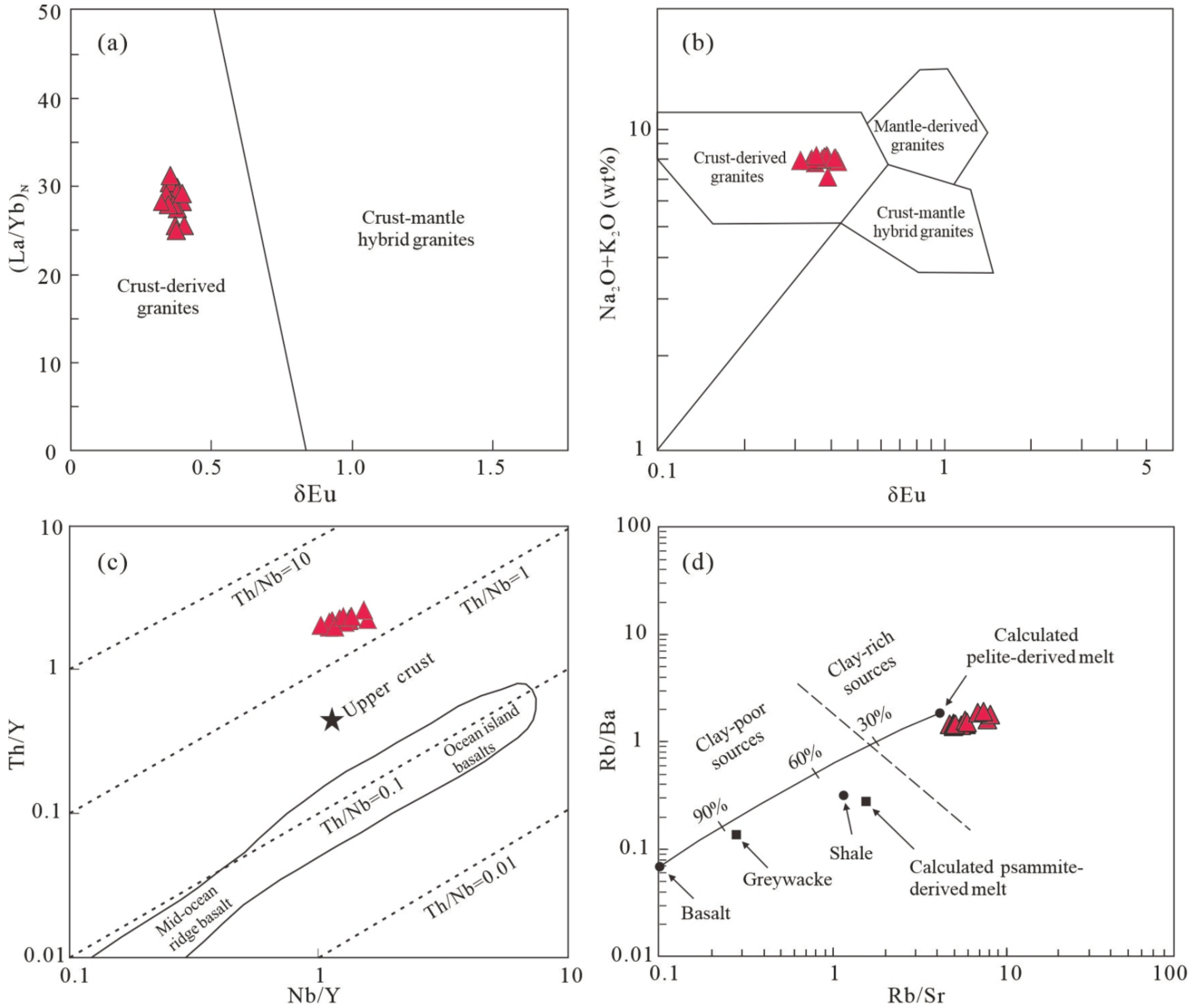


**Fig. 7** Discrimination diagrams of magma source for the Wutang granites. (**a**) δEu−(La/Yb)N diagram (after Zhang et al., 2014). (**b**) δEu−($Na_2O$+$K_2O$) diagram (after Chappell, 1999). (**c**) Nb/Y−Th/Y diagram (after Boztuğ et al., 2007). (**d**) Rb/Sr−Rb/Ba diagram (after Sylvester, 1998)

Ba diagram (Fig. 7d), all samples are projected into the field of clay-rich sources and at the endmember of pelite-derived melt. This also indicates that the magma originated from the partial melting of pelites. In conclusion, the magma of the Wutang granites originated from the partial melting of ancient crustal materials dominated by metamorphosed pelites.

### 5.4 Geodynamic setting

As discussed earlier, the Wutang granites belong to peraluminous S-type granites. Such granites generally result from the partial melting of thickened crust and can form either in a compressional setting during collision orogeny or in an extensional setting following peak collision (Kalsbeek 2001; Lin and Ma 2003; Zhang et al. 2012a; Li et al. 2020). In the diagrams of R1−R2 (Fig. 9a) and (Y+Nb)−Rb (Fig. 9b), the samples are plotted in the transitional field between the syn-collision and post-orogenic or post-collision granites. Correspondingly, the samples are plotted in the transitional field between the compressional- and extensional-type granites in the $SiO_2$−lg[CaO/($Na_2O$+$K_2O$)] diagram (Fig. 9c). These tectonic discrimination diagrams indicate that the Wutang granites were formed in a transitional setting from compression to extension.

The South China Plate was formed through the collision of the Yangtze and Cathaysia Blocks along the Jiangnan orogenic belt during the Neoproterozoic (Zhang and Zheng 2013; Shu et al. 2021). Numerous studies have revealed that the South

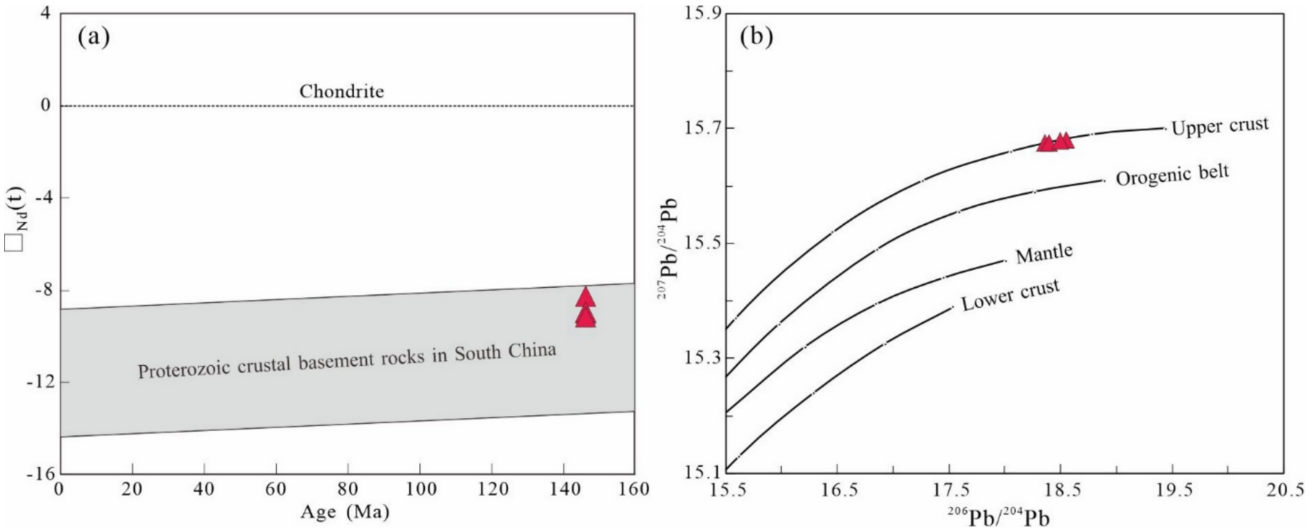


**Fig. 8** (**a**) Relationship between age and εNd(t) values of the Wutang granites (after Zhang et al., 2022). (**b**) 206Pb/204Pb−207Pb/204Pb diagram of the Wutang granites (after Zartman and Doe, 1981)

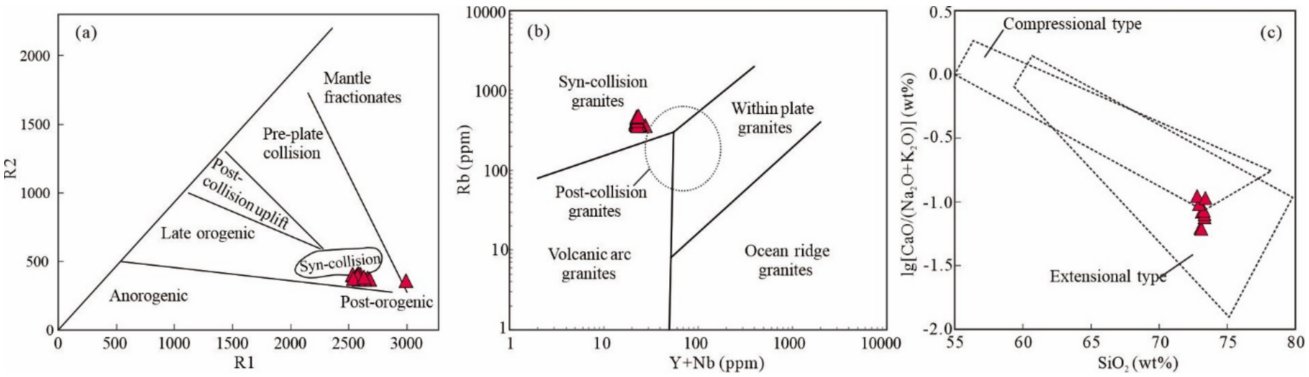


**Fig. 9** Discrimination diagrams of the tectonic setting for the Wutang granites. (**a**) R1−R2 diagram (after Batchelor and Bowden, 1985). (**b**) (Y+Nb)−Rb diagram (after Pearce et al., 1984). (**c**) SiO2−lg[CaO/(Na2O+K2O)] (Brown, 1982)

China Plate has been influenced by the episodic subduction of the Paleo-Pacific Plate since the Early Jurassic (Zhang et al. 2009; Yan et al. 2011; Yang and He 2013; Meng et al. 2015; Shu et al. 2020; Zhu et al. 2020; Lü et al. 2023), and it underwent multiple episodes of lithospheric extension during the Middle Jurassic to the Late Cretaceous (Li 1999; Xie 2003; Mao et al. 2004, 2007; Hu et al. 2007; Ni et al. 2023). The subduction triggered crustal uplift and subsequent denudation, resulting in the general absence of Middle-Late Jurassic strata in the South China Plate (Zhang et al. 2012b; Chu et al. 2019). Regionally, the Late Jurassic strata are absent. Fluvial and lacustrine sediments (e.g., the Lengshuiwu Formation), representing an extensional tectonic setting, did not occur until the late Early Cretaceous (Zhou et al. 2025). Furthermore, previous studies have demonstrated that the entire northern Jiangxi Province, including the study region, underwent intense compression during the Middle-Late Jurassic period (ca. 172–157 Ma), as evidenced by the large-scale folds and thrust-nappe structures (e.g., the thrust fault system in the Jingdezhen area) during this period (Huo et al. 2018; Hu 2023). By the Early Cretaceous period (< 135 Ma), the formation of faulted depression basins (e.g., the Poyang Lake Basin) in northern Jiangxi Province, signifies that the regional tectonic evolution had progressed to the extensional phase (Shu et al. 2009; Yang et al. 2016). Meanwhile, some Early Cretaceous magmatic rocks in the region, including rhyolites from the Daguding and Ehuoling Formations and granites from the Lingshan, Hengshan, and Yunshan plutons, have been confirmed to have formed in an extensional setting (Wu et al. 2016; Wang et al. 2019; Tian et al. 2021; Yu et al. 2023). The aforementioned stratigraphic, tectonic, and magmatic evidence implies that the regional tectonic regime might have transformed from compression to extension during the late Jurassic to the early Cretaceous. The Wutang granites have a

monazite U–Pb age of 145.8 ± 1.0 Ma (Fig. 3b), suggesting that they were emplaced during this tectonic transition period. In summary, the Wutang granites in the TBMD were generated in a compression-extension transitional setting related to the episodic subduction of the Paleo-Pacific Plate.

## 6 Conclusions

(1) The Wutang pluton consists of medium- to fine-grained two-mica monzogranites, with a monazite U–Pb age of 145.8 ± 1.0 Ma.
(2) The petrographic, geochemical, and Nd–Pb isotopic features indicate that the Wutang granites belong to highly fractionated S-type granites, and their magma was derived from the partial melting of ancient crustal materials dominated by metamorphosed pelites.
(3) The Wutang granites formed in a compression-extension transitional setting related to the episodic subduction of the Paleo-Pacific Plate.

**Acknowledgements** Special appreciation to Editorial Director Binbin Wang for his time and efforts in enhancing our manuscript. We also appreciate the anonymous reviewers' insightful comments, which improved the quality of this manuscript. We are grateful to the experts at the State Key Laboratory of Nuclear Resources and Environment of the East China University of Technology, the Nanchang Mineral Resources Supervision and Testing Center of the Ministry of Land and Resources of China, and the Wuhan Center of China Geological Survey for their assistance with sample analysis and data processing.

**Author contributions** Fushen Zhang and Xiaotian Zhang conceived and wrote the manuscript; Fangrong Zhang, Zhe Xu, Xinyu Xu, Yu Zhou, Ying Liu, and Longmin Nie provided samples and designed experiments; Guoqi Liu and Fujun Zhong performed experiments and data processing; Yong Zhang, Jiayong Pan, and Fei Xia contributed to the design, coordination, and finalization of the manuscript.

**Funding** This study was funded by the Program of Science and Technology Department of Jiangxi Province (2023KDG01002 and 2023KDG01003), the National Natural Science Foundation of China (42062006 and 41962007), the Key Research and Development Program of Jiangxi Province (20223BBG71015), and the Personnel Training Project of Jiangxi Bureau of Geology (2023JXDZKJRC02, 2022JXDZKJRC04, and 2024JXDZKJRC05).

**Data availability** The authors confirm that the data supporting the findings of this study are available in the manuscript. The data in this study are unpublished and have not been submitted to any other journal for review.

**Code availability** There is no software application or custom code in this manuscript.

**Declarations**

**Conflict of interest** On behalf of all authors, the corresponding author states that there is no conflict of interest.

**Human and animal rights** This manuscript does not involve any human or animal experiments. Our study adhered to scientific ethical standards and complied with the current laws of the country in which it was conducted.

**Consent for publication** This manuscript contains no individual data in any form. All authors gave their consent for publication.

## References

Ballouard C, Poujol M, Boulvais P, Branquet Y, Tartèse R, Vigneresse JL (2016) Nb-Ta fractionation in peraluminous granites: a marker of the magmatic-hydrothermal transition. Geology 44(3):231–234. https://doi.org/10.1130/g37475.1

Batchelor RA, Bowden P (1985) Petrogenetic interpretation of granitoid rock series using multicationic parameters. Chem Geol 48(1–4):43–55. https://doi.org/10.1016/0009-2541(85)90034-8

Bau M (1996) Controls on the fractionation of isovalent trace elements in magmatic and aqueous systems: evidence from Y/Ho, Zr/Hf, and lanthanide tetrad effect. Contrib Mineral Petrol 123(3):323–333. https://doi.org/10.1007/s004100050159

Boztuğ D, Harlavan Y, Arehart GB, Satır M, Avcı N (2007) K-Ar age, whole-rock and isotope geochemistry of A-type granitoids in the Divriği-Sivas region, eastern-central Anatolia, Turkey. Lithos 97(1–2):193–218. https://doi.org/10.1016/j.lithos.2006.12.014

Brown GC (1982) Calc-alkaline intrusive rocks: their diversity, evolution and relation to arcs. In: Thorpe RS (ed) Andesites-orogenic andesites and related rocks. John Wiley and Sons, New York, pp 437–464

Chappell BW (1999) Aluminium saturation in I- and S-type granites and the characterization of fractionated haplogranites. Lithos 46(3):535–551. https://doi.org/10.1016/S0024-4937(98)00086-3

Chappell BW, White AJR (2001) Two contrasting granite types: 25 years later. Aust J Earth Sci 48(4):489–499. https://doi.org/10.1046/j.1440-0952.2001.00882.x

Chen J, Wang RC, Zhu JC, Lu JJ, Ma DS (2013) Multiple-aged granitoids and related tungsten-tin mineralization in the Nanling Range, South China. Sci China Earth Sci 56(12):2045–2055. https://doi.org/10.1007/s11430-013-4736-9

Chen XY, Wu JH, Tang WX, Xie CH, Gong M, Wang GH, Zhou XG, Gao Y, Zhou XJ, Deng MC, Li YJ, Nie XL, Lai CJ, Zhang FS, Li RZ, Zhang JQ, Wei JH (2023) Newly found giant granite-associated lithium resources in the western Jiangxi Province, South China. Earth Sci 48(10):3957–3960. https://doi.org/10.3799/dqkx.2023.189

Chu PL, Duan Z, Liao SB, Huang WC, Hong WT, Zhu YH, Shu XJ (2019) Petrogenesis and tectonic significances of Late Mesozoic granitoids in the Dahutang area, Jiangxi Province: constraints from zircon U-Pb dating, mineral-chemistry, geochemistry and Hf isotope. Acta Geol Sin 93(7):1687–1707. https://doi.org/10.19762/j.cnki.dizhixuebao.2019053

Collins WJ, Beams SD, White AJR, Chappell BW (1982) Nature and origin of A-type granites with particular reference to southeastern Australia. Contrib Mineral Petrol 80(2):189–200. https://doi.org/10.1007/BF00374895

Duan Z, Xing GF, Liao SB, Chu PL, Huang WC, Zhu YH (2017) Compositional difference from the sources of Jiuling Neoproterozoic granite complex in Eastern Segment of the Jiangnan Orogen: Constraints from geochemistry and Hf isotope of zircons. Acta Petrol Sin 33(11):3610–3634

El Bouseily AM, El Sokkary AA (1975) The relation between Rb, Ba and Sr in granitic rocks. Chem Geol 16(3):207–219. https://doi.org/10.1016/0009-2541(75)90029-7

Galer SJG (1998) Practical application of lead triple spiking for correction of instrumental mass discrimination. Mineral Mag 62A(1):491–492. https://doi.org/10.1180/minmag.1998.62a.1.260

Gonçalves GO, Lana C, Scholz R, Buick IS, Gerdes A, Kamo SL, Corfu F, Marinho MM, Chaves AO, Valeriano C, Nalini HA (2016) An assessment of monazite from the Itambé pegmatite district for use as U-Pb isotope reference material for microanalysis and implications for the origin of the "Moacyr" monazite. Chem Geol 424:30–50. https://doi.org/10.1016/j.chemgeo.2015.12.019

Gonçalves GO, Lana C, Scholz R, Buick IS, Gerdes A, Kamo SL, Corfu F, Rubatto D, Wiedenbeck M, Nalini HA Jr, Oliveira LCA (2018) The Diamantina monazite: a new low-Th reference material for microanalysis. Geostand Geoanal Res 42(1):25–47. https://doi.org/10.1111/ggr.12192

Gou SL, Yu JH, Cai YF, Jiang W, Mao ZQ (2023) Distribution and enrichment mechanism of lithium in meta-sedimentary rocks in the Jiangnan orogen and implications for lithium mineralization. Acta Geol Sin 97(11):3696–3724. https://doi.org/10.19762/j.cnki.dizhixuebao.2023260

Green TH (1995) Significance of Nb/Ta as an indicator of geochemical processes in the crust-mantle system. Chem Geol 120(3–4):347–359. https://doi.org/10.1016/0009-2541(94)00145-X

Hou ZD, Zhao Z, Liu ZJ, Wang JP (2023) Metallogenetic regularity and prospecting direction of granite related Li-Be-Nb-Ta deposits in the Nanling region, South China. Acta Petrologica Sinica 39:1950–1972 (in Chinese with English abstract)

Hu RZ, Bi XW, Peng JT, Liu S, Zhong H, Zhao JH, Jiang GH (2007) Some problems concerning relationship between Mesozoic-Cenozoic lithospheric extension and uranium metallogenesis in South China. Miner Depos 26(2):139–152. https://doi.org/10.3969/j.issn.0258-7106.2007.02.001

Hu XC, Yang ZX, Kang WL, Guo XG, Chen HY, Lei ZQ, Liu YB, Gong ZZ, Jing DL (2023) Zircon U-Pb age, geochemical characteristics and its geological significance of the Qianhongquan monzonite in Beishan area, Gansu province. Mineral Petrol 43(4):49–59. https://doi.org/10.19719/j.cnki.1001-6872.2023.04.05

Hu BJ (2023) Mesozoic tectonic-magmatic evolution of the eastern part of Pingxiang-Leping depression and its adjacent areas (PhD thesis). University of Geosciences, Beijing. China. pp. 210

Hua RM, Li GL, Zhang WL, Hu DQ, Chen PR, Chen WF, Wang XD (2010) A tentative discussion on differences between large-scale tungsten and tin mineralizations in South China. Miner Depos 29(1):9–23. https://doi.org/10.16111/j.0258-7106.2010.01.005

Huo HL, Zhang D, Chen ZL, Bi MF, Chen GH, He XL, Li N, Li XJ, Xue W, Ouyang YP (2018) Deformation characteristics and geochronological constraints of Mesozoic nappe structure in Jingdezhen area, northeastern Jiangxi. J Geomech 24(1):9–24. https://doi.org/10.12090/j.issn.1006-6616.2018.24.01.002

Jian KK, Liu XD, He YF, Yuan Z, Zeng ZC, Zhao DC, Wang X, Du B, Wang TY (2018) Geochronology, geochemistry and petrogenesis of the Datonggou granitic plutons in the middle section of Altun Mountains. Geol China 45(4):740–752. https://doi.org/10.12029/gc20180407

Kalsbeek F, Jepsen HF, Nutman AP (2001) From source migmatites to plutons: Tracking the origin of ca. 435 Ma S-type granites in the east Greenland Caledonian Orogen. Lithos 57(1):1–21. https://doi.org/10.1016/S0024-4937(00)00071-2

King PL, White AJR, Chappell BW, Allen CM (1997) Characterization and origin of aluminous A-type granites from the Lachlan fold belt, southeastern Australia. J Petrol 38(3):371–391. https://doi.org/10.1093/petroj/38.3.371

Koester E, Pawley AR, Fernandes LAD, Porcher CC, Soliani E (2002) Experimental melting of cordierite gneiss and the petrogenesis of syntranscurrent peraluminous granites in southern Brazil. J Petrol 43(8):1595–1616. https://doi.org/10.1093/petrology/43.8.1595

Lan HF, Wang HZ, Ling HF, Chen WF, Wang KX, Wang D (2020) Petrogenesis of the Chashan granite in the northern Guangdong Province and its implication for the metallogenic potential of tungsten and uranium mineralization. Acta Geol Sin 94(4):1143–1165. https://doi.org/10.19762/j.cnki.dizhixuebao.2020022

Li XH (1999) Cretaceous magmatism and lithosphere extension in South China: The geochronology and geochemistry constraints. Resource Environment and Sustaining Development. Science Press, Beijing, pp 264–275

Li RZ, Zhou ZB, Peng B, Chen J, Wu JB, Yu HQ, Wan JJ, Yang S (2020) A discussion on geological characteristics and genetic mechanism of Dagang superlarge lithium-bearing porcelain stone deposit in Yifeng County, Jiangxi Province. Miner Depos 39(6):1015–1029. https://doi.org/10.16111/j.0258-7106.2020.06.004

Li XF, Wei XL, Zhu YT, Li ZF, Deng XC (2021) Rare metal deposits in South China: Types, characteristics, distribution and tectonic setting. Acta Petrologica Sinica 37:3591-3614 (in Chinese with English abstract)

Liang X, Xu YJ, Zi JW, Zhang HC, Du YS (2022) Genetic mineralogy of monazite and constraints on interpretation of U-Th-Pb ages. Earth Sci 47(4):1383–1398

Lin GC, Ma CQ (2003) Genesis of peraluminous granitoids and their tectonic settings. Geol Miner Resour South China 19(1):65–70

Linnen RL, Lichtervelde MV, Cerny P (2012) Granitic pegmatites as sources of strategic metals. Elements 8:275–280

Liu Y, Gao S, Hu Z, Gao C, Zong K, Wang D (2010) Continental and oceanic crust recycling-induced melt-peridotite interactions in the Trans-North China Orogen: U-Pb dating, Hf isotopes and trace elements in zircons from mantle xenoliths. J Petrol 51(1–2):537–571. https://doi.org/10.1093/petrology/egp082

Liu BQ, Yu JH, Jiang W, Cai YF (2023) Geochemistry of the meta-sedimentary rocks of the Shuangqiaoshan Group and their genetic link to tungsten mineralization in northern Jiangxi, South China. Acta Geol Sin 97(2):433–447. https://doi.org/10.19762/j.cnki.dizhixuebao.2022229

Lou FS, Xu Z, Huang H, Xiong YY (2023) Geological characteristics and prospecting significance of low grade super large granite mica-type lithium deposits in Jiangxi Province. J East China Univ Technol Nat Sci 46(5):425–436. https://doi.org/10.3969/j.issn.1674-3504.2023.05.001

Lü XH, Wang GG, Ni P (2023) Reworking of continental crust and the large-scale Cu and W mineralization in the northern Jiangxi part of the Jiangnan Orogen. Bull Mineral Petrol Geochem 42(5):1132–1149. https://doi.org/10.19658/j.issn.1007-2802.2023.42.102

Lu YF, Li WX (2021) Calculation method and VBA program of CIPW norm minerals. South China Geol 37(3):348–360. https://doi.org/10.3969/j.issn.2097-0013.2021.03.009

Ludwig KR (2003) Isoplot 3.0: a geochronological toolkit for microsoft excel. Berkeley Geochronology Center Special Publication, Berkeley

Maniar PD, Piccoli PM (1989) Tectonic discrimination of granitoids. Geol Soc Am Bull 101(5):635–643

Mao JW, Xie GQ, Li XF, Zhang CQ, Mei YX (2004) Mesozoic large scale mineralization and multiple lithospheric extension in South China. Earth Sci Front 11(1):45–55

Mao JW, Xie GQ, Guo CL, Chen YC (2007) Large-scale tungsten-tin mineralization in the Nanling region, South China: Metallogenic ages and corresponding geodynamic processes. Acta Petrol Sin 23(10):2329–2338. https://doi.org/10.3969/j.issn.1000-0569.2007.10.002

Mao JW, Ouyang H, Song SW, Santosh M, Yuan SD, Zhou ZH, Zheng W, Liu H, Liu P, Cheng YB, Chen MH (2019) Geology and metallogeny of tungsten and tin deposits in China. Mineral

Deposits of China. Society of Economic Geologists, pp411–482. https://doi.org/10.5382/sp.22.10
Meng LF, Li ZX, Chen HL, Li XH, Zhu C (2015) Detrital zircon U-Pb geochronology, Hf isotopes and geochemistry constraints on crustal growth and Mesozoic tectonics of southeastern China. J Asian Earth Sci 105:286–299. https://doi.org/10.1016/j.jseaes.2015.01.015
Middlemost EAK (1994) Naming materials in the magma/igneous rock system. Earth Sci Rev 37(3–4):215–224. https://doi.org/10.1016/0012-8252(94)90029-9
Nakada S, Takahashi M (1979) Regional variation in chemistry of the miocene intermediate to felsic magmas in the outer zone and the Setouchi province of southwest Japan. Geol Soc Jap 85:571–582.
Ni P, Pan JY, Han L, Cui JM, Gao Y, Fan MS, Li WS, Chi Z, Zhang KH, Cheng ZL (2023) Large-scale granite-related tungsten and tin mineralization in South China: temporal and spatial distribution, metallogenic models and exploration implications. Acta Geol Sin 97(11):3497–3544. https://doi.org/10.19762/j.cnki.dizhixuebao.2023368
Nie XL, Wang SL, Liu S, Xu L (2022) Geological and geochemical characteristics of the Xikeng lithium deposit and the $^{40}Ar/^{39}Ar$ chronology of lepidolite of the deposit in Jiangxi Province, China. Acta Mineral Sin 42(3):285–294. https://doi.org/10.16461/j.cnki.1000-4734.2022.42.039
Pearce JA, Harris NBW, Tindle AG (1984) Trace element discrimination diagrams for the tectonic interpretation of granitic rocks. J Petrol 25(4):956–983. https://doi.org/10.1093/petrology/25.4.956
Peccerillo A, Taylor SR (1976) Geochemistry of Eocene calc-alkaline volcanic rocks from the Kastamonu area, Northern Turkey. Contrib Mineral Petrol 58(1):63–81. https://doi.org/10.1007/BF00384745
Rong W (2017) A geochemical study of Neoproterozoic granites from the Jiuling Range in South China (PhD dissertation). University of Science and Technology of China, Hefei. pp.1–219.
Rudnick RL, Fountain DM (1995) Nature and composition of the continental crust: a lower crustal perspective. Rev Geophys 33(3):267–309. https://doi.org/10.1029/95rg01302
Shu LS, Zhou XM, Deng P, Wang B, Jiang SY, Yu JH, Zhao XX (2009) Mesozoic tectonic evolution of the southeast China Block: new insights from basin analysis. J Asian Earth Sci 34(3):376–391. https://doi.org/10.1016/j.jseaes.2008.06.004
Shu LS, Chen XY, Lou FS (2020) Pre-Jurassic tectonics of the South China. Acta Geol Sin 94(2):333–360. https://doi.org/10.19762/j.cnki.dizhixuebao.2020046
Shu LS, Yao JL, Wang B, Faure M, Charvet J, Chen Y (2021) Neoproterozoic plate tectonic process and Phanerozoic geodynamic evolution of the South China Block. Earth Sci Rev 216:103596. https://doi.org/10.1016/j.earscirev.2021.103596
Sun SS, McDonough WF (1989) Chemical and isotopic systematics of oceanic basalts: implications for mantle composition and processes. Geol Soc Lond Spec Publ 42(1):313–345. https://doi.org/10.1144/GSL.SP.1989.042.01.19
Sylvester PJ (1998) Post-collisional strongly peraluminous granites. Lithos 45(1–4):29–44. https://doi.org/10.1016/S0024-4937(98)00024-3
Taylor SR, McLennan SM (1995) The geochemical evolution of the continental crust. Rev Geophys 33(2):241–265. https://doi.org/10.1029/95rg00262
Tian MM, Li ZY, Nie JT, Liu JG, Wang J, Cao JH (2021) A comparative study and its genesis of porphyroclastic rhyolite from ehuling and daguding formations in Midwestern of Xiangshan uranium orefield, Jiangxi Province. Earth Sci 46(12):4546–4561.
Wang D, Wang XL, Cai Y, Chen X, Zhang FR, Zhang FF (2017) Heterogeneous conservation of zircon xenocrysts in Late Jurassic granitic intrusions within the Neoproterozoic Jiuling Batholith, South China: a magma chamber growth model in deep crustal hot zones. J Petrol 58(9):1781–1810. https://doi.org/10.1093/petrology/egx074
Wang CZ, Huang ZZ, Xing GF, Zhao XL, Shu XJ, Ju DM (2019) Petrogenesis of the Yunshan pluton in Jiangxi Province: Constrains from geochronology, geochemistry and Nd-Hf isotopes. Acta Geol Sin 93(5):1055–1068. https://doi.org/10.19762/j.cnki.dizhixuebao.2019049
Watson EB, Harrison TM (1983) Zircon saturation revisited: temperature and composition effects in a variety of crustal magma types. Earth Planet Sci Lett 64(2):295–304. https://doi.org/10.1016/0012-821X(83)90211-X
Whalen JB (1985) Geochemistry of an island-arc plutonic suite: The Uasilau-Yau Yau intrusive complex, New Britain, PNG. J Petrol 26(3):603–632. https://doi.org/10.1093/petrology/26.3.603
Whalen JB, Currie KL, Chappell BW (1987) A-type granites: geochemical characteristics, discrimination and petrogenesis. Contrib Mineral Petrol 95(4):407–419. https://doi.org/10.1007/BF00402202
Wu FY, Li XH, Yang JH, Zheng YF (2007) Discussions on the petrogenesis of granites. Acta Petrol Sin 23(6):1217–1238. https://doi.org/10.3969/j.issn.1000-0569.2007.06.001
Wu WW, Liao QA, Chen S, Hu CB, Tian J, Wang FM, Fan GM (2015) Petrogenesis and geological significance of highly fractionated A-type granites in Kalasayi, East Junggar. Geol Bull China 34(S1):385–399. https://doi.org/10.3969/j.issn.1671-2552.2015.02.016
Wu XL, Fan XJ, Gong ZY, Xiao X, Hua X, Fang JH (2016) Geological characteristics and genesis of the Lingshan complex in Jiangxi Province. Geol J China Univ 22(3):459–466. https://doi.org/10.16108/j.issn1006-7493.2015221
Wu FY, Liu XC, Ji WQ, Wang JM, Yang L (2017) Highly fractionated granites: recognition and research. Sci China Earth Sci 60(7):1201–1219. https://doi.org/10.1007/s11430-016-5139-1
Wu FY, Guo CL, Hu FY, Liu XC, Zhao JX, Li XF, Qin KZ (2023a) Petrogenesis of the highly fractionated granites and their mineralizations in Nanling Range, South China. Acta Petrol Sin 39(1):1–36. https://doi.org/10.18654/1000-0569/2023.01.01
Wu QH, Zhou HX, Liu B, Kong H, Pei JY, Qin YX, Zong Q, Wu KY, Tang YY (2023b) Spatio-temporal distribution of granite-related rare metal deposits and W-Sn deposits in South China and their genetic relationship. Bull Geol Sci Technol 42(1):78–88. https://doi.org/10.19509/j.cnki.dzkq.2022.0047
Xie GQ (2003) Geological and geochemical characteristics of the Late Mesozoic basic dikes (bodies) in SE China and their geodynamic significance: A case study of Jiangxi Province (PhD thesis). Institute of Geochemistry, Chinese Academy of Sciences. pp128.
Xie L, Liu Y, Wang RC, Hu H, Che XD, Xiang L (2019) Li–Nb–Ta mineralization in the Jurassic Yifeng granite-aplite intrusion within the Neoproterozoic Jiuling Batholith, South China: A fluid-rich and quenching ore-forming process. J Asian Earth Sci 185:104047. https://doi.org/10.1016/j.jseaes.2019.104047
Xu XB, Xue DJ, Li Y, Hu P, Chen NS (2014) Neoproterozoic sequences along the Dexing-Huangshan fault zone in the eastern Jiangnan orogen, South China: Geochronological and geochemical constrains. Gondwana Res 25(1):368–382. https://doi.org/10.1016/j.gr.2013.03.020
Xu B, Jiang SY, Wang R, Ma L, Zhao KD, Yan X (2015) Late Cretaceous granites from the giant Dulong Sn-polymetallic ore district in Yunnan Province, South China: Geochronology, geochemistry, mineral chemistry and Nd–Hf isotopic compositions. Lithos 218:54–72. https://doi.org/10.1016/j.lithos.2015.01.004
Xu WT, Zhang XH, Zhang BB, Lyu JS, Sun JD, Zhang Y, Wu B (2022) Genesis of highly fractionated S-type granites: Evidence from zircon U-Pb age, Hf isotopes and geochemistry of

Fuquanshan pluton, northeastern Jiangxi Province. Geol Bull China 41(4):577–589.

Xu Z, Zhang Y, Pan JY, Zhang FS, Xia F, Wu ZC, Han SC, Liu GQ, Zhong FJ, Zhang XT, Liu Y, Yan J, Zhang FR (2023) *In situ* LA–ICP–MS analyses of muscovite: constraints on granite-type Li mineralization in northwestern Jiangxi, South China. Ore Geol Rev 156:105402. https://doi.org/10.1016/j.oregeorev.2023.105402

Xu Z, Zhang FR, Zhang FS, Wang GH, Wu JH, Tang WX, Lou FS, Xie CH, Gao Y, Dong J, Chen J, Kuang EL, Zhou B (2024) Metallogenic geological characteristics and prospecting direction of altered granite-type lithium deposit in southern margin of Jiuling, Jiangxi Province. Miner Depos 43(2):244–264. https://doi.org/10.16111/j.0258-7106.2024.02.002

Yan Y, Hu XQ, Lin G, Santosh M, Chan LS (2011) Sedimentary provenance of the Hengyang and Mayang basins, SE China, and implications for the Mesozoic topographic change in South China Craton: evidence from detrital zircon geochronology. J Asian Earth Sci 41(6):494–503. https://doi.org/10.1016/j.jseaes.2011.03.012

Yang ZY, He B (2013) Transform of Jurassic tectonic configuration of South China Block: evidence from U-Pb ages of detrital zircons. Geotectonica Metallog 37(4):580–591. https://doi.org/10.16539/j.ddgzyckx.2013.04.013

Yang XD, Wu ZH, Zhang HJ (2016) Geological evolution, neotectonics and genetic mechanism of the Poyang Lake Basin. J Geomech 22(3):667–684. https://doi.org/10.3969/j.issn.1006-6616.2016.03.021

Yang F (2019) Highly fractionated granite: mineral, geochemical features and their implications (Master thesis). China University of Geosciences, Beijing. pp83.

Yang WP, Li CL, Yang YJ, Fu AZ, Zheng B, Zhou TF, Zhao RJ (2023) Geochemistry, petrogenesis and tectonic setting of the Middle Jurassic taxi plutons in Heilongjiang. Geoscience 37(2):390–403. https://doi.org/10.19657/j.geoscience.1000-8527.2021.158

Yu Q, Chen YL, Chen ZH, Liao HB (2023) LA-ICP-MS zircon U-Pb age, geochemistry and genesis of the Hengshan granite in Wulijie, northern Jiangxi Province. J East China Univ Technol Nat Sci 46(3):239–258. https://doi.org/10.3969/j.issn.1674-3504.2023.03.005

Zaraisky GP, Aksyuk AM, Devyatova VN, Udoratina OV, Chevychelov VY (2009) The Zr/Hf ratio as a fractionation indicator of rare-metal granites. Petrology 17(1):25–45. https://doi.org/10.1134/S0869591109010020

Zartman RE, Doe BR (1981) Plumbotectonics: the model. Tectonophysics 75(1–2):135–162. https://doi.org/10.1016/0040-1951(81)90213-4

Zhang SB, Zheng YF (2013) Formation and evolution of Precambrian continental lithosphere in South China. Gondwana Res 23(4):1241–1260. https://doi.org/10.1016/j.gr.2012.09.005

Zhang YQ, Xu XB, Jia D, Shu LS (2009) Deformation record of the change from Indosinian collision-related tectonic system to Yanshanian subduction-related tectonic system in South China during the Early Mesozoic. Earth Sci Front 16(1):234–247. https://doi.org/10.3321/j.issn:1005-2321.2009.01.026

Zhang Q, Ran H, Li CD (2012a) A-type granite: What is the essence? Acta Petrol Mineral 31(4):621–626.

Zhang YQ, Dong SW, Li JH, Cui JJ, Shi W, Su JB, Li Y (2012b) The new progress in the study of Mesozoic tectonics of South China. Acta Geosci Sin 33(3):257–279. https://doi.org/10.3975/cagsb.2012.03.01

Zhang SZ, Li FQ, Li Y, Liu W, Qin YD (2014) Early Ordovician strongly peraluminous granite in the middle section of the Yarlung Zangbo junction zone and its geological significance. Sci China Earth Sci 57(4):630–643. https://doi.org/10.1007/s11430-013-4721-3

Zhang FS, Xu J, Zhang J, Guo JS (2020) Geochemical characteristics, zircon U-Pb age and geological significance of new Proterozoic granites in Jiuling area, Jiangxi Province. J East China Univ Technol Nat Sci 43(1):12–20. https://doi.org/10.3969/j.issn.1674-3504.2020.01.002

Zhang FS, Xu J, Feng GS (2021a) Comprehensive survey and evaluation of Chinastone resources in the Yifeng—Fengxin area of Yichun City, Jiangxi Province. Jiangxi Geological Survey Research Institute. 1–91.

Zhang XT, Sun JG, Han JL, Feng YY (2021b) Genesis and ore-forming process of the Benqu mesothermal gold deposit in the Jiapigou ore cluster, NE China: constraints from geology, geochronology, fluid inclusions, and whole-rock and isotope geochemistry. Ore Geol Rev 130:103956. https://doi.org/10.1016/j.oregeorev.2020.103956

Zhang YQ, Ding JL, Gao Q, Zhou P, Zeng ZJ, Li ZL (2022) Petrogenesis of granites in Dachen island, Zhejiang Province: Constraints from geochemistry, zircon U-Pb ages and Sr-Nd-Hf isotopes. Geol Bull China 41(10):1798–1812. https://doi.org/10.12097/j.issn.1671-2552.2022.10.009

Zhao KD, Jiang SY (2022) How to form the famous South China W-Sn province? Earth Sci 47(10):3882–3884. https://doi.org/10.3799/dqkx.2022.849

Zhou JT, Luo W, Xiong R, Xiao YB, Zhang FS, Qiu WJ (2025) Diagenetic and metallogenic geological background of the lithium deposits in the Yifeng-Fengxin lithium ore field on the southern edge of Jiuling Mountain. Chin J Geol 60(1):229–249.

Zhu QB, Jin GD, Gao TS (2020) Study and geological implication of detrital zircons in Shuibei Formation of Early Jurassic in Zhangshudun of northeastern Jiangxi Province. Geol Surv China 7(5):42–53. https://doi.org/10.19388/j.zgdzdc.2020.05.06